Title

Cyclic Avian Mass Mortality in the Northeastern United States Is Associated with a Novel Orthomyxovirus

Journal

Journal of Virology, 89(2)

ISSN

0022-538X

Authors

Allison, Andrew B
Ballard, Jennifer R
Tesh, Robert B
et al.

Publication Date

2015-01-15

DOI

10.1128/jvi.02019-14

Peer reviewed

JVI
Journals.ASM.org

Cyclic Avian Mass Mortality in the Northeastern United States Is Associated with a Novel Orthomyxovirus

Andrew B. Allison,[a,b] Jennifer R. Ballard,[b] Robert B. Tesh,[c] Justin D. Brown,[b] Mark G. Ruder,[b] M. Kevin Keel,[b] Brandon A. Munk,[b] Randall M. Mickley,[d] Samantha E. J. Gibbs,[e] Amelia P. A. Travassos da Rosa,[c] Julie C. Ellis,[f] Hon S. Ip,[g] Valerie I. Shearn-Bochsler,[g] Matthew B. Rogers,[h] Elodie Ghedin,[h] Edward C. Holmes,[i] Colin R. Parrish,[a] Chris Dwyer[j]

Baker Institute for Animal Health, Department of Microbiology and Immunology, College of Veterinary Medicine, Cornell University, Ithaca, New York, USA[a]; Southeastern Cooperative Wildlife Disease Study, College of Veterinary Medicine, University of Georgia, Athens, Georgia, USA[b]; Department of Pathology, Center for Biodefense and Emerging Infectious Diseases, University of Texas Medical Branch, Galveston, Texas, USA[c]; United States Department of Agriculture, Animal and Plant Health Inspection Service, Wildlife Services, MA/CT/RI Program, Sutton, Massachusetts, USA[d]; United States Department of the Interior, United States Fish and Wildlife Service, Patuxent Research Refuge, Laurel, Maryland, USA[e]; Department of Infectious Disease and Global Health, Cummings School of Veterinary Medicine, Tufts University, North Grafton, Massachusetts, USA[f]; United States Geological Survey, National Wildlife Health Center, Madison, Wisconsin, USA[g]; Department of Computational and Systems Biology, Center for Vaccine Research, University of Pittsburgh, Pittsburgh, Pennsylvania, USA[h]; Marie Bashir Institute for Infectious Diseases and Biosecurity, Charles Perkins Centre, School of Biological Sciences and Sydney Medical School, University of Sydney, Sydney, NSW, Australia[i]; United States Department of the Interior, United States Fish and Wildlife Service, Northeast Region, Division of Migratory Birds, Hadley, Massachusetts, USA[j]

ABSTRACT

Since 1998, cyclic mortality events in common eiders (*Somateria mollissima*), numbering in the hundreds to thousands of dead birds, have been documented along the coast of Cape Cod, MA, USA. Although longitudinal disease investigations have uncovered potential contributing factors responsible for these outbreaks, detecting a primary etiological agent has proven enigmatic. Here, we identify a novel orthomyxovirus, tentatively named Wellfleet Bay virus (WFBV), as a potential causative agent of these outbreaks. Genomic analysis of WFBV revealed that it is most closely related to members of the *Quaranjavirus* genus within the family *Orthomyxoviridae*. Similar to other members of the genus, WFBV contains an alphabaculovirus gp64-like glycoprotein that was demonstrated to have fusion activity; this also tentatively suggests that ticks (and/or insects) may vector the virus in nature. However, in addition to the six RNA segments encoding the prototypical structural proteins identified in other quaranjaviruses, a previously unknown RNA segment (segment 7) encoding a novel protein designated VP7 was discovered in WFBV. Although WFBV shows low to moderate levels of sequence similarity to *Quaranfil virus* and *Johnston Atoll virus*, the original members of the *Quaranjavirus* genus, additional antigenic and genetic analyses demonstrated that it is closely related to the recently identified Cygnet River virus (CyRV) from South Australia, suggesting that WFBV and CyRV may be geographic variants of the same virus. Although the identification of WFBV in part may resolve the enigma of these mass mortality events, the details of the ecology and epidemiology of the virus remain to be determined.

IMPORTANCE

The emergence or reemergence of viral pathogens resulting in large-scale outbreaks of disease in humans and/or animals is one of the most important challenges facing biomedicine. For example, understanding how orthomyxoviruses such as novel influenza A virus reassortants and/or mutants emerge to cause epidemic or pandemic disease is at the forefront of current global health concerns. Here, we describe the emergence of a novel orthomyxovirus, Wellfleet Bay virus (WFBV), which has been associated with cyclic large-scale bird die-offs in the northeastern United States. This initial characterization study provides a foundation for further research into the evolution, epidemiology, and ecology of newly emerging orthomyxoviruses, such as WFBV, and their potential impacts on animal and/or human health.

Between 1998 and 2013, 12 mortality events were documented in common eiders (*Somateria mollissima*) along the coast of Cape Cod, MA, USA. The number of sick or dead eiders observed during these outbreaks typically averaged between 200 and 600 birds; however, a mortality event involving approximately 3,000 eiders was documented from August to October 2007. The underlying causes of recent large-scale mortality events are unclear, although periodic anecdotal die-offs of eiders in Massachusetts have been reported since the 1950s (1). Cape Cod is a major wintering ground for common eiders (2), with most birds arriving from various northeastern United States and Canadian colonies in the early fall, with a small resident (year-round) population that also inhabits the area. While late-winter/early-spring mortality events have been observed in some instances, most die-offs appear to begin in late summer/early fall, suggesting a seasonal occurrence of disease that may coincide with the arrival (and/or buildup) of

Received 14 July 2014 **Accepted** 7 November 2014

Accepted manuscript posted online 12 November 2014

Citation Allison AB, Ballard JR, Tesh RB, Brown JD, Ruder MG, Keel MK, Munk BA, Mickley RM, Gibbs SEJ, Travassos da Rosa APA, Ellis JC, Ip HS, Shearn-Bochsler VI, Rogers MB, Ghedin E, Holmes EC, Parrish CR, Dwyer C. 2015. Cyclic avian mass mortality in the northeastern United States is associated with a novel orthomyxovirus. J Virol 89:1389–1403. doi:10.1128/JVI.02019-14.

Editor: A. García-Sastre

Address correspondence to Andrew B. Allison, aba75@cornell.edu.

Supplemental material for this article may be found at http://dx.doi.org/10.1128/JVI.02019-14.

doi:10.1128/JVI.02019-14

migrating birds. During field investigations of these outbreaks, most of the affected eiders were found dead. However, moribund birds in different stages of illness have also been observed, and these exhibited a variety of premonitory clinical signs, including lethargy, incoordination, respiratory distress, diarrhea, and convulsions. Despite active multi-institutional investigations of these outbreaks identifying potential complicating factors of the mortality events, including emaciation and heavy burdens of parasitic worms (acanthocephalans), no primary pathogen was identified in sick or dead eiders that could explain these reoccurring die-offs. Currently, no other species (avian or otherwise) has been observed to show similar clinical signs of disease, although other sympatric bird species, such as mergansers, scoters, and gulls, have been present in low to moderate numbers during eider outbreaks; whether the disease is host restricted to common eiders is uncertain.

In October 2010, a mass mortality event occurred in Wellfleet Harbor, Cape Cod, Barnstable County, MA, USA, from which we collected eider carcasses for postmortem examination. At necropsy, common gross lesions included moderate to severe emaciation and parasitism with acanthocephalans and cestodes, similar to that observed in previous outbreaks. Although parasite infestations in these birds appeared to be a commonly observed condition, the various degrees of parasites among the affected birds, along with the recognition of heavy parasite burdens in asymptomatic eiders, suggested these infestations were likely to be an incidental or contributing factor rather than the driver of the observed morbidity and mortality. Indeed, heavy parasite burdens were found in most eiders sampled, irrespective of health status, similar to that observed in other studies (3). Although many of the birds examined had moderate to severe coagulative necrosis in a number of different organs, the most prominent lesions were often observed in the liver, from which a virus was isolated in multiple birds. Here, we describe this virus that, based on genetic, antigenic, and phylogenetic analysis, is determined to be a novel orthomyxovirus. The virus was tentatively named Wellfleet Bay virus (WFBV), in relation to the area of Cape Cod (Wellfleet Bay Harbor) where the 2010 outbreak occurred.

The *Orthomyxoviridae* family has historically consisted of five genera: *Influenza virus A*, *B*, and *C*, along with *Isavirus* and *Thogotovirus*, which differ in their host ranges and routes of transmission (4). While natural transmission of *Influenza A virus* (FLUAV) in the avian reservoir (waterfowl, shorebirds) is believed to be through the fecal-oral route (5), transmission in humans occurs predominately through respiratory aerosols/droplets and by direct contact (6, 7). Both *Influenza B virus* (FLUBV) and *Influenza C virus* (FLUCV) are respiratory-borne human viruses that (in the case of FLUCV) can infect other mammals, such as swine, but unlike FLUAV do not naturally circulate in birds (8). The genus *Isavirus* currently comprises a single species, *Infectious salmon anemia virus* (ISAV), that infects fish and is believed to be water transmitted or possibly vectored by sea lice (9), as well as being transmitted vertically (10). The genus *Thogotovirus* currently consists of two approved species, *Thogoto virus* (THOV) and *Dhori virus* (DHOV) (4, 11, 12), both of which predominately infect mammals and are tick-borne (13, 14).

In contrast to the influenza viruses and ISAV, the surface glycoprotein (GP) of the tick-borne thogotoviruses shares identity to the gp64 protein of group I alphabaculoviruses, which is a low-pH-activated class III fusion protein involved in virus entry and cell-cell fusion (15–17). Viruses of the family *Baculoviridae* (double-stranded DNA [dsDNA] viruses) predominately infect members of the order Lepidoptera (moths and butterflies) (18) but have also been isolated from Diptera (mosquitoes) (19) and Hymenoptera (sawflies, wasps) (20). Although the origin of the acquisition of the gp64-like protein by thogotoviruses remains obscure, it is theorized to be the functional catalyst for their ability to infect and be transmitted by ticks (21). The target host receptor/ligand for the gp64-like protein of any of the tick-borne orthomyxoviruses, as with the alphabaculoviruses, is currently unknown, although direct interaction of gp64 with membrane phospholipids prior to low-pH-induced hemifusion and pore formation has recently been suggested (22).

In 2011, a new genus denoted *Quaranjavirus* was proposed to the ICTV and subsequently ratified, which included two new species, *Quaranfil virus* (QRFV) and *Johnston Atoll virus* (JAV), and a tentative member, Lake Chad virus (LKCV). Although these three viruses were only recently recognized as orthomyxoviruses (23), they were originally isolated in the 1950s and 1960s: QRFV in Quaranfil, Egypt, in 1953; JAV in Sand Island, Johnston Atoll, in the North Pacific, in 1964; and LKCV in Lake Chad, Nigeria, in 1969 (24, 25). The geographic distribution of QFRV appears to be widespread, stretching across Africa, the Middle East, and Asia (26, 27), as does JAV, which in addition to Johnston Atoll has been reportedly isolated in Hawaii (28), Australia (29), and New Zealand (30). In contrast, the natural distribution of LKCV is unknown, as its geographical range can only be inferred from the single isolation of the prototype strain in Nigeria (23).

Similar to the thogotoviruses, the quaranjaviruses contain a gp64-like surface glycoprotein (denoted hemagglutinin [HA] based on its ability to agglutinate erythrocytes at low pH rather than having any sequence homology to the cognate influenza protein), suggesting a close phylogenetic relationship between the two genera (4). However, unlike THOV and DHOV that primarily circulate in transmission cycles involving hard ticks (family Ixodidae) and mammals (14), the quaranjaviruses appear to predominately cycle in soft ticks (family Argasidae) and aquatic birds (23). As soft ticks are often found in tropical and subtropical habitats that contain very high population densities of nesting birds (31, 32), the quaranjaviruses have been associated primarily with colonial nesting species, such as gannets, terns, and herons, or other communal birds, such as weavers (23, 25, 30, 33).

In 2010, a new orthomyxovirus designated Cygnet River virus (CyRV) was isolated during an outbreak of fatal disease in captive Muscovy ducks (*Cairina moschata*) on Kangaroo Island, South Australia (34). Remarkably, although the outbreak sites are approximately 17,000 km apart, genetic and antigenic comparisons between WFBV and CyRV (as shown here) demonstrate they may be geographical variants of the same virus. Here, we biologically, genetically, and antigenically characterize WFBV, investigate its relationship to the newly discovered CyRV, and explore the evolution and natural history of the quaranjaviruses as a whole.

MATERIALS AND METHODS

Gross and microscopic analysis of common eiders. On 25 October 2010, an outbreak of disease in common eiders was investigated by USDA Wildlife Services personnel along Jeremy Point, Wellfleet Harbor, Cape Cod, Barnstable County, MA, USA. Seven moribund birds, in various stages of disease, were humanely euthanized, and their carcasses were shipped on ice to the SCWDS for diagnostic evaluation. Routine postmortem gross

and microscopic examination was conducted on the eider carcasses. Samples of all major organs, and any observed lesions in additional tissues, were collected in 10% buffered formalin. Fixed tissues were routinely processed for histology, embedded in paraffin, sectioned at 3 to 5 μm, and stained with hematoxylin and eosin. Special stains and bacterial cultures were performed as indicated.

Virus isolation and identification. Samples (~0.5 cm^3) of brain, heart, liver, spleen, kidney, lung, bursa of Fabricius, and gastrointestinal tract from seven affected birds were mechanically homogenized in 650 μl of minimum essential medium (MEM) supplemented with 10% fetal bovine serum (FBS), 400 units/ml penicillin, 400 μg/ml streptomycin, and 1 μg/ml amphotericin B (Sigma-Aldrich, St. Louis, MO). Homogenized tissues were centrifuged (6,700 × *g* for 10 min), and clarified supernatant (100 μl) was used to infect 2-day-old 4.0-cm^2 confluent monolayers of Vero E6 and Pekin duck embryo (PDE) cells. Cell lines were obtained from the American Type Culture Collection (ATCC; Manassas, VA). Cultures were passaged at 7- to 10-day intervals. For wells exhibiting cytopathology, virus was harvested and amplified once in Vero E6 cells for generation of stock virus. The isolates were then tested biochemically using diethyl ether, 5-bromo-2′-deoxyuridine (Sigma-Aldrich), and by stepwise 0.2- to 0.1-μm-pore-size filtration (Whatman; Maidstone, Kent, United Kingdom) to tentatively assess the physical nature of the virus particle (presence/absence of an envelope, nucleic acid composition, particle size). To enrich the level of viral nucleic acid in the extraction sample, multiple confluent 75-cm^2 flasks of Vero E6 cells were infected at a multiplicity of infection (MOI) of 1.0, and supernatant was recovered at day 4 postinfection and pooled. Virus was precipitated overnight at 4°C with 7% polyethylene glycol (PEG) 6000 and 2.3% NaCl and pelleted by centrifugation at 13,000 × *g* for 1 h. The pellet was resuspended in 1 ml of TES buffer (10 mM Tris-Cl [pH 7.4], 2 mM EDTA, 150 mM NaCl) and centrifuged (13,000 × *g*, 15 min) to remove the PEG. Viral nucleic acids were extracted from the supernatant using a QIAamp viral RNA minikit (Qiagen, Valencia, CA), and cDNA was amplified with random primers using an ImPromp-II reverse transcription (RT)-PCR system (Promega, Madison, WI). Amplicons were cloned using a PCR cloning kit (Qiagen) and sequenced using plasmid-specific primers.

Ultrathin-section transmission electron microscopy. Virus-infected Vero E6 and baby hamster kidney (BHK) cells were fixed in 2.5% formaldehyde and 0.1% glutaraldehyde containing 0.03% trinitrophenol and 0.03% $CaCl_2$ in 0.05 M cacodylate buffer. Cells were harvested, pelleted, postfixed in 1% OsO_4 in 0.1 M cacodylate buffer, stained *en bloc* with 2% aqueous uranyl acetate, dehydrated in ethanol, and embedded in Poly/Bed 812 (Polysciences, Warrington, PA). Ultrathin sections were cut on a Reichert-Leica Ultracut S ultramicrotome, stained with 0.4% lead citrate, and visualized with a Philips 201 electron microscope at 60 kV (FEI Company, Hillsboro, OR).

Negative-stain transmission electron microscopy. To obtain high concentrations of virus for visualization by electron microscopy, virus was propagated in Vero E6 cells and PEG precipitated as noted above. Formvar-coated 400-mesh copper specimen grids (Electron Microscopy Sciences, Hatfield, PA) were then floated on enriched virus in TES buffer spotted on Parafilm, wicked dry, and negatively stained with 2% potassium phosphotungstate, pH 7.0, for 1 min. Negatively stained virions were visualized using a JEOL JEM 1210 transmission electron microscope at 120 kV (JEOL Limited, Tokyo, Japan).

Anti-WFBV polyclonal antibody production. Mouse hyperimmune ascites fluid (MHIAF) was generated against WFBV isolate 10-280-G using protocols previously reported (35). Immunogens used for antibody production consisted of 10% suspensions of brain tissue derived from intracerebrally infected 2-day-old newborn mice in phosphate-buffered saline (PBS) mixed with an equal volume of Freund's adjuvant just prior to inoculation. The immunization schedule consisted of four intraperitoneal injections given at weekly intervals. To induce ascites formation, sarcoma 180 cells were also given intraperitoneally after the final immunization. All animal experiments were carried out under protocols approved by the University of Texas Medical Branch IACUC.

Antigenic analysis. The antigenic relationship of WFBV to other orthomyxoviruses was assessed by complement fixation (CF) tests as described previously (35). Antigens and antibodies were prepared as noted above. CF microtiter tests were conducted using two full units of guinea pig complement. Titers were recorded as the highest antibody dilution giving 3+ or 4+ fixation of complement on a scale of 0 to 4+, where 0 indicates complete hemolysis and 4+ indicates no hemolysis.

Immunohistochemistry of naturally infected eiders. Tissue sections from clinically ill eiders, from which virus was isolated, were analyzed by immunohistochemistry (IHC) to determine if tissue lesions correlated with the presence of WFBV antigen. Briefly, formalin-fixed paraffin-embedded tissues were deparaffinized in xylene and rehydrated in successive decreasing ethanol washes (100, 95, 70%). Slides were then treated with 3% hydrogen peroxide to quench endogenous peroxidase activity. Endogenous biotin and avidin were blocked in successive steps (biotin blocking system; Dako, Carpinteria, CA). Antigen retrieval was performed with proteinase K (Dako, Carpinteria, CA), and to prevent nonspecific protein binding, a commercial blocking reagent was applied (Power Block universal blocking reagent; BioGenex, San Ramon, CA). Slides were incubated in a 1:7,000 dilution of anti-WFBV MHIAF. Bound antibody was detected using a 1:100 dilution of a biotinylated horse anti-mouse secondary antibody (Vector, Burlingame, CA), followed by horseradish peroxidase-labeled streptavidin (Biocare, Concord, CA) and 3,3′-diaminobenzidine (DAB) as the chromogen (Dako, Carpinteria, CA). Slides were counterstained with hematoxylin and then dehydrated and mounted for microscopic evaluation.

Genomic sequencing. WFBV isolate 10-280-G was used as a template for genomic sequencing. Virus was propagated in Vero E6 cells, PEG precipitated, and then purified on a 20% sucrose cushion followed by a 30 to 60% sucrose gradient in a Beckman SW 32 Ti rotor at 134,000 × *g* for 4 h at 4°C using an Optima L-100K ultracentrifuge (Beckman Coulter, Brea, CA) (36). The virus band was recovered by side puncture and concentrated with an Amicon Ultra-15 100K centrifugal filter unit (Millipore, Billerica, MA), and viral RNA was extracted as previously noted. Extracted RNA was then used to generate a cDNA library. Briefly, an Illumina sequencing library was prepared using TruSeq RNA-seq library preparation kit v2 (Illumina, San Diego, CA), without the initial poly(A) isolation and starting with chemical fragmentation of the RNA. All subsequent steps were conducted according to the manufacturer's protocol. Clustering was performed using TruSeq PE cluster kit v3, and data were collected from a single lane on a HiSeq 2000 instrument using TruSeq SBS kit v3. A paired-end, 2 × 100-bp sequencing run was performed twice with HiSeq control software v1.5.15.1, and base calling was performed using RTA v1.13.48, with phasing and prephasing values from a control PhiX lane on the same flow cell. *De novo* assembly of the WFBV genome from the paired-end reads was performed using Velvet (37) and IDBA-UD (38) assemblers. Terminal ends of the genome were confirmed by rapid amplification of cDNA ends (RACE) using a FirstChoice RLM-RACE kit (Life Technologies).

Bioinformatic analysis. Molecular masses and isoelectric points for WFBV proteins were predicted using the ProtParam tool on the ExPASy server (http://web.expasy.org/protparam/). Signal peptides and transmembrane domains were predicted using the Phobius server (http://phobius.sbc.su.se). Potential conserved motifs in WFBV proteins were identified by a motif scan analysis using the Hits database on the Swiss Institute of Bioinformatics (SIB) server (http://myhits.isb-sib.ch/cgi-bin/motif_scan). Nucleotide and protein similarities were assessed using NCBI BLAST (http://blast.ncbi.nlm.nih.gov/Blast.cgi) and the Max Planck Institute Bioinformatics toolkit (http://toolkit.tuebingen.mpg.de) servers (39).

Mass spectrometry. To obtain viral proteins for mass spectrometry, WFBV purified on a sucrose gradient was mixed with 5× Laemmli sample buffer (250 mM Tris-HCl [pH 6.8], 25% β-mercaptoethanol, 10% SDS,

50% glycerol, 0.05% bromophenol blue) and boiled for 5 min. Proteins were electrophoresed by SDS-PAGE in a 10% polyacrylamide gel and stained with a SYPRO ruby protein gel stain (Molecular Probes, Invitrogen, Carlsbad, CA) and/or a Pierce silver stain kit (Thermo Scientific). Molecular masses were estimated against a Precision Plus protein dual-color standards ladder (Bio-Rad, Hercules, CA). Viral proteins in the SYPRO ruby-stained gel were then excised using a UV transilluminator and subjected to nanoscale high-performance liquid chromatography coupled to tandem mass spectrometry (nano HPLC-MS/MS) as previously described (40). Briefly, proteins were reduced with 10 mM dithiothreitol, alkylated with 55 mM iodoacetamide, and digested overnight with 0.5 μg trypsin. Tryptic peptides were centrifuged (4,000 × *g*, 2 min), and the remaining peptides in the gel were sonicated in 50% acetonitrile-5% formic acid and collected. Pooled tryptic peptides were evaporated in a Speedvac SC110 (ThermoSavant, Milford, MA, USA), reconstituted in 2% acetonitrile-0.5% formic acid, and analyzed with nano HPLC-MS/MS using an LTQ-Orbitrap Elite mass spectrometer (Thermo Fisher Scientific, San Jose, CA). Proteins were identified by searching MS/MS spectra using the MascotDaemon search engine (version 2.3.02; Matrix Science, Boston, MA) against a combination database of *Chlorocebus aethiops* from NCBI and the seven identified WFBV proteins. Search settings for Mascot included tryptic peptide specificity of one missed cleavage site, Asn/Gln deamidation and methionine oxidation as variable modifications, and carbamidomethyl cysteine as a fixed modification. Proteins identified by MS/MS were filtered with the false discovery rate of detected tryptic peptides at ~1% using a decoy database search in Mascot.

Molecular modeling. The three-dimensional structure of the WFBV HA was predicted using the Protein Homology/AnalogY Recognition Engine 2 (Phyre2) Web-based server available at http://www.sbg.bio.ic.ac.uk/phyre2 (41). Secondary structures, regions of disorder, and putative homologous domains in the WFBV HA to other known proteins were predicted using the Intensive Modeling option in Phyre2. The template sequence/structure used to create the WFBV HA protein model was the crystal structure of the postfusion form of the alphabaculovirus gp64 from *Autographa californica nucleopolyhedrovirus* (AcMNPV) (PDB 3DUZ) (17).

Cloning of the WFBV genome. To facilitate the future development of a reverse genetics system for WFBV, the seven genomic segments of WFBV 10-280-G were cloned. All cloned segments were sequenced confirmed against the assembled genome to ensure they contained no additional mutations. RNA segments were amplified using primers that contained the terminal conserved residues along with enough 3′ primer sequence to specifically amplify the desired segment (primer sequences available upon request). cDNA amplicons of each RNA segment were generated using a SuperScript III one-step RT-PCR system with Platinum *Taq* (Invitrogen, Carlsbad, CA), and products were TA cloned into a pDRIVE vector (Qiagen) according to the manufacturer's protocol.

Fusion assays. To test if the HA of WFBV had fusogenic activity similar to that of gp64, fusion assays were developed using both live virus (10-280-G) and a plasmid construct containing the HA of 10-280-G. For the development of the HA plasmid construct, the HA segment was amplified from pDRIVE using primers containing HindIII/BamHI restriction sites and subcloned into pcDNA 3.1(−) (Invitrogen) to create pcDNA3.1-10-280G-HA. Vero E6 cells (~60% confluent) in a 10.0-cm^2-well format were then transfected with 2.0 μg of pcDNA3.1-10-280G-HA using Lipofectamine 2000 (Invitrogen) according to the manufacturer's protocol. At days 4 and 5 posttransfection, standard MEM (pH 7.4) supplemented with 5% FBS was removed, cells were washed 2× in sterile PBS and incubated in MEM adjusted to pH 4.0 for 10 min, and then the acidic medium was removed and replaced with standard MEM. Cells were monitored hourly for syncytium formation. For fusion assays with live virus, the same protocol was used, except cells were infected with WFBV 10-280-G at an MOI of 2 and assayed at days 3 and 4 postinfection. Controls consisted of pH 4.0-treated noninfected cells and cells transfected with empty pcDNA 3.1(−). Expression of HA in transfected cells was confirmed by immunoblotting using WFBV MHIAF according to standard methods (42).

***In vitro* host range.** In addition to Vero E6 and PDE cells, the ability of WFBV to replicate in various host cells was assessed using the mammalian cell lines: (i) A-549 (human lung carcinoma), (ii) LLC-MK2 (rhesus monkey [*Macaca mulatta*] kidney epithelium), (iii) RF/6A (rhesus monkey retinal endothelium), (iv) CPAE (cattle [*Bos taurus*] pulmonary artery endothelium), (v) OK (Virginia opossum [*Didelphis virginiana*] kidney), (vi) Tb 1 Lu (Mexican free-tailed bat [*Tadarida brasiliensis*] lung epithelium), and (vii) Mv 1 Lu (American mink [*Neovison vison*] lung epithelium), the avian cell line QNR/K2 (Japanese quail [*Coturnix japonica*] Müller cells), and the mosquito cell line C6/36 (Asian tiger mosquito [*Aedes albopictus*] larvae). All cell lines were obtained from the ATCC and were grown in MEM supplemented with 2.2 g/liter $NaHCO_3$, 5% FBS, 400 units/ml penicillin, 400 μg/ml streptomycin, and 1 μg/ml amphotericin B. Cells were maintained at 28°C (mosquito) or 37°C (avian and mammalian) in a humidified atmosphere containing 5% CO_2. Cells were infected at an MOI of 0.2 in a 4.0-cm^2-well format, and wells were harvested daily for 6 days and frozen at −80°C for subsequent multistep growth curve analysis. Titrations were performed on Vero E6 cells overlaid with 1% gum tragacanth/1× MEM supplemented with 3% FBS. Cultures were inactivated on day 14 postadsorption with 10% buffered formalin and stained with 0.25% crystal violet for plaque visualization. Dilutions in which 20 to 100 plaques could be counted (when applicable) were used in determining titers ($\log_{10}$ PFU/ml).

Phylogenetic analysis. As PB1 is the most conserved protein among the various orthomyxovirus genera (43), it was used in determining the evolutionary relationship of WFBV to other orthomyxoviruses. To this end, we collated the full-length PB1 amino acid sequences of 18 additional orthomyxoviruses representing five genera within the family (genus *Isavirus* was omitted due to lack of viable alignment; see the Fig. 7 legend for a full list of viruses) and aligned them to WFBV using MUSCLE (44) assuming default parameters. Because of the highly divergent nature of the sequence alignment, all ambiguously aligned regions and all gapped sites were pruned prior to phylogenetic analysis using Gblocks (45). This resulted in a final sequence alignment of 378 conserved amino acid residues from 19 viruses. Note that the LCKV PB1 sequence (GenBank accession number FJ861698) was omitted from the analysis due to its truncated length. To infer the evolutionary relationships among these sequences, we utilized the maximum likelihood (ML) method available within PhyML package version 3.0 (46), assuming the WAG+Γ model of amino acid substitution and a combination of both nearest neighbor interchange (NNI) and subtree pruning and regrafting (SPR) branch swapping. To determine support for individual nodes, we performed a bootstrap resampling analysis using 1,000 replicate ML trees (parameters as described above).

In an attempt to resolve the phylogenetic position of WFBV with more precision, we performed a second phylogenetic analysis on the full-length PB1 of members of the genus *Quaranjavirus* (JAV, QRFV, WFBV), including the recently characterized Tyulek ("Tjuloc") virus (TLKV) (47), in isolation. In this case, the sequence alignment was 766 amino acid residues in length. Additionally, a phylogenetic analysis of all available putative M proteins of the quaranjaviruses (CyRV, QRFV, TLKV, WFBV) was undertaken, resulting in a sequence alignment of 264 amino acids. These analyses proceeded in the same manner as that described above, although the strong similarity among the four viruses in each case meant that Gblocks pruning was not required.

Nucleotide sequence accession numbers. The complete genome of WFBV has been deposited in GenBank under the accession numbers KM114304 to KM114310.

RESULTS

Clinical signs during the outbreak. Clinical signs observed in moribund birds during the disease investigation in 2010 at Jeremy Point in Wellfleet Harbor included diarrhea, lethargy, and recum-

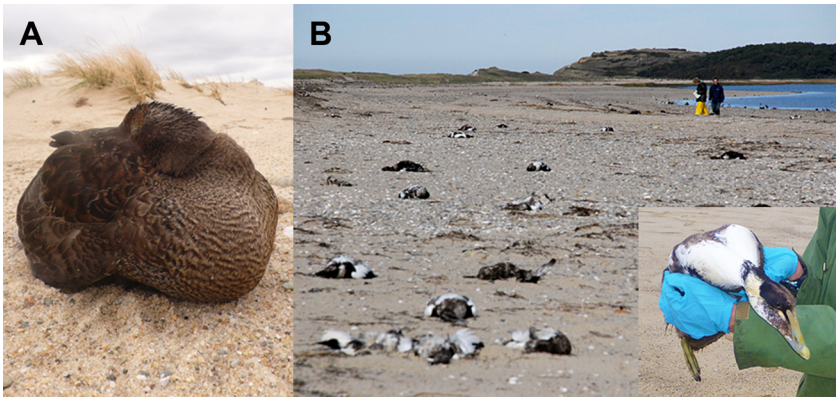

FIG 1 Morbidity and mortality of common eiders in association with natural WFBV infection in Cape Cod, MA, USA. (A) Morbid female eider displaying reversed head posture and extreme lethargy, common clinical signs in WFBV-infected birds. (B) Multi-institutional disease investigation of a mass die-off during 2006. Hundreds to thousands of dead eiders have been documented during such cyclic outbreaks, which generally appear annually during the fall. Inset, WFBV-infected birds such as this male eider (sexes are dimorphic) exhibit listlessness and recumbency and are easily captured. (Photo B courtesy of Jim Canavan, Woods Hole Oceanographic Institution.)

bency. Many affected birds were found listless and rested their heads backwards onto their bodies (Fig. 1) or on the sand without attempting to escape from capture when approached. Individual birds that attempted to escape capture ran and flapped their wings futilely but tired quickly and were easily caught, demonstrating they were significantly weakened. Herring gulls (*Larus smithsonianus*) were observed to be feeding on dead eiders in the vicinity; however, no dead or moribund gulls were noted. Seven moribund eiders were humanely euthanized, and their carcasses were shipped overnight on ice for diagnostic evaluation.

Gross and microscopic analysis of common eiders. The seven eiders submitted for necropsy included male and female birds of various ages (i.e., juvenile and adult). All birds were moderately to severely emaciated, weighing between 1.0 and 1.6 kg (normal weights for both sexes are between 1.2 and 3.1 kg) (48), and were assessed to be in poor nutritional condition based on a prominent keel (i.e., pectoral muscle atrophy) and lack of subcutaneous or visceral adipose tissue. Other gross findings included multifocal lesions on the serosal and cut surfaces of the liver (Fig. 2A) and mild to severe acanthocephalan (parasitic spiny-headed worms of

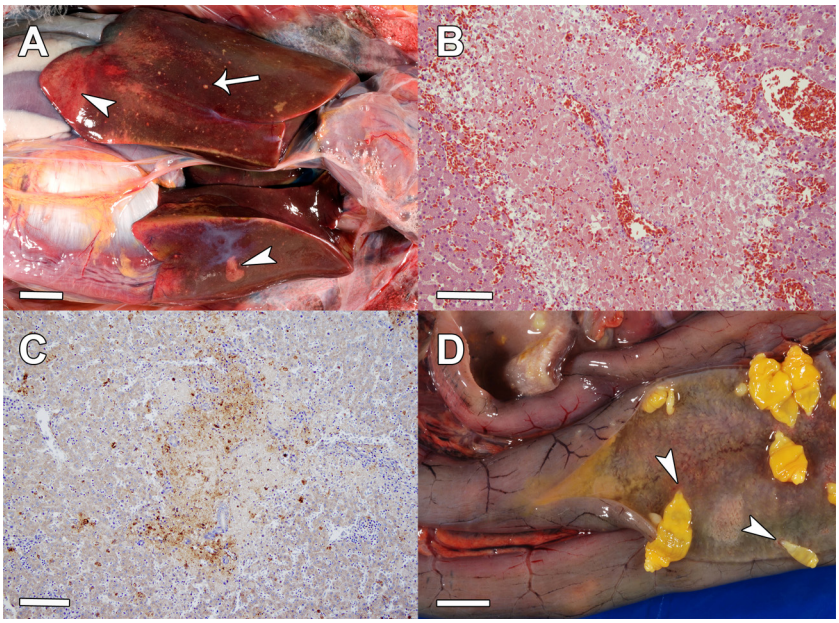

FIG 2 Gross and histopathological lesions associated with natural WFBV infection in common eiders. (A) Coelomic cavity of a WFBV-infected eider. The liver contains coalescing to focally extensive (arrowheads) and multifocal (arrow) white to tan lesions on the serosal and cut surfaces. Scale bar = 1 cm. (B) Microscopic view of a liver lesion, characterized by variably sized areas of acute hepatocellular necrosis and hemorrhage. Scale bar = 100 μm. (C) Colocalization of WFBV antigen and pathological lesions. Eiders that were observed showing clinical signs of disease, and from which virus was isolated, were tested for viral antigen by immunohistochemistry using anti-WFBV mouse hyperimmune ascites fluid. Viral antigen was detected in hepatocellular lesions using DAB chromogen (shown as reddish-brown precipitate). Scale bar = 100 μm. (D) Acanthocephalan infection in the intestinal tract of a common eider infected with WFBV. The intestine has been cut transversely to display the yellow spiny-headed worms of the phylum Acanthocephala that are ubiquitous enteric parasites of common eiders. Note the attachment of the proboscis to the intestinal wall (arrowheads) and associated inflammation. Scale bar = 0.5 cm.

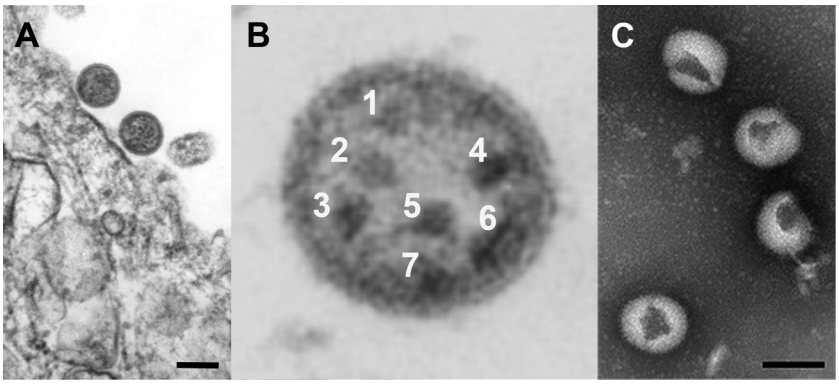

FIG 3 Transmission electron microscopy of WFBV. (A) Ultrathin-section micrograph of two virions budding from the surface of infected Vero E6 cells. Scale bar = 100 nm. (B) Transversely sectioned virion (~100 nm in diameter) from infected BHK cells, apparently showing seven ribonucleoprotein complexes. (C) Virions negatively stained with 2% potassium phosphotungstate, pH 7.0, with protruding hemagglutinin (HA) glycoproteins visible on the surface. Magnification = ×60,000. Scale bar = 100 nm.

the phylum Acanthocephala) infestations in the gastrointestinal tract (Fig. 2D). Microscopic diagnosis for each bird varied, but consistent histopathological findings in most eiders included moderate to severe, acute multifocal to coalescing necrosis with variable lymphoplasmacytic hepatitis and hemorrhage in the liver (Fig. 2B), renal hemorrhage, along with mild to severe, chronic, multifocal to diffuse acanthocephaliasis with variable necrosis in the intestines.

Virus isolation and identification. A presumptive enveloped RNA virus (i.e., 5-bromo-2′-deoxyuridine resistant, diethyl ether sensitive) with a particle size of ≥ 100 nm (based on titer reduction following 100-nm filtration) was isolated from four of the seven birds (10-280-A, -B, -C, -G) submitted to the SCWDS for necropsy. The virus induced cytopathology in both cell lines used for isolation (Vero E6 and PDE cells), although cytopathic effects were characterized largely by the lack of discrete plaque formation or cell detachment and by extensive cellular vacuole formation. Virus was recovered from the liver only in each of the four 2010 cases, and in conjunction with the severe lesions routinely observed in the liver, this suggested that the virus may be hepatotropic or that the liver may serve as a major site of replication. However, it should be noted that we have isolated the virus from additional tissues (i.e., spleen, intestines, kidney) collected from eiders in both subsequent (2011, 2012, 2013) and former (2007, 2009) outbreaks, suggesting infection is likely systemic. These findings also indicate that the virus has repeatedly been recovered from sick or dying birds in multiple years, suggesting that the 2010 die-off was not an isolated event.

Cultures of Vero E6 cells were subsequently used for further virus preparations/stocks, as they were shown to grow virus to higher titers ($10^{8.02}$ PFU/ml) than other cell lines tested (see "Experimental host range"). For each of four isolates (10-280-A, -B, -C, -G), RNA was extracted and used as the template in RT-PCR. Protein BLAST analysis of cDNA clones randomly amplified from viral RNA demonstrated the highest identity to QRFV and JAV in a number of proteins (polymerase acidic [PA], polymerase basic 1 [PB1], polymerase basic 2 [PB2], and hemagglutinin [HA] proteins). This represented the first molecular identification of the virus, suggesting it was a previously unknown member of the genus *Quaranjavirus*, family *Orthomyxoviridae*. Additionally, another clone determined to be of viral origin (i.e., primer sequences were made from the clone to verify the sequence could be detected only in infected cells) could not be identified by database searches. This clone was later determined to be the newly discovered seventh RNA segment by searching the Illumina reads using this sequence (see "Genomic sequencing"). All four viruses were shown to be the same virus species. Based on the origin of where the birds were recovered (Wellfleet Bay Harbor, Cape Cod, MA), the virus was tentatively named Wellfleet Bay virus (WFBV).

Other than the noted acanthocephalans and light growth of *Staphylococcus saccharolyticus* and *Fusobacterium* spp. in anaerobic culture of liver from eider 10-280-C, no other parasitic, viral, or bacterial pathogens or environmental toxins were detected in eider tissues by routine methods.

Thin-section transmission electron microscopy. Ultrathin sections of WFBV-infected Vero E6 and BHK cells demonstrated particles approximately 90 to 110 nm in diameter, consistent with the known particle size of other orthomyxoviruses (80 to 120 nm) (4). In some instances, virions of WFBV could be observed budding from plasma membranes (Fig. 3A). Interestingly, certain transverse sections of virions in which ribonucleoproteins (RNPs) could be visualized suggested that seven RNPs were present in virions (Fig. 3B), reaffirming the presence of at least seven strands of negative-sense RNA composing the WFBV genome (see "Genomic sequencing").

Negative-stain transmission electron microscopy. In virus preparations that were negatively stained with 2% potassium phosphotungstate (pH 7.0), virions of approximately 90 to 110 nm in diameter were observed. These virions appeared to be exclusively spherical or ovoid and did not exhibit pleomorphic shapes. Dark stains present in virions were likely artifacts due to penetration of potassium phosphotungstate into ruptured particles (Fig. 3C). WFBV virions were morphologically very similar to virions of CyRV (34).

Antigenic analysis. Complement fixation tests using WFBV MHIAF and antigen were performed against other orthomyxoviruses, including those in the *Quaranjavirus*, *Thogotovirus*, and *Influenzavirus A* genera. WFBV MHIAF was shown to react with its homologous antigen (WFBV 10-280-G), as well as to CyRV antigen. However, it did not cross-react with antigens derived from any other members of the *Quaranjavirus* genus, including QRFV, JAV, LKCV, or TLKV, or with members of *Thogotovirus* (Table 1)

TABLE 1 Antigenic comparisons of WFBV against all known or suspected tick-borne orthomyxoviruses by complement fixation testing

	Titer[a]											
	Antibody (genus *Quaranjavirus*)						Antibody (genus *Thogotovirus*)					
Antigen	WFBV	CyRV	QRFV	JAV	LKCV	TLKV	ABV	UPOV	ARAV	DHOV	THOV	JOSV
WFBV	512/≥16	512/≥16	0	0	0	0	0	0	0	0	0	0
CyRV	512/≥16	512/≥16	0	0	0	0	0	0	0	0	0	0
Normal	0	0	0	0	0	0	0	0	0	0	0	0
Homologous			64/32	128/≥8	≥256/≥8	1024/128	≥64/≥8	≥64/≥8	≥64/≥8	≥256/≥8	≥256/≥8	≥64/≥8

[a] Complement fixation results are expressed as highest reciprocal antibody dilution/highest reciprocal antigen dilution showing reactivity, where 0 = <8/<8.

or *Influenzavirus A* (not shown). Complement fixation titers with WFBV MHIAF were indistinguishable when using WFBV or CyRV as the antigen. The reciprocal tests using CyRV MHIAF against the panel of antigens yielded identical results, with CyRV MHIAF cross-reacting with only WFBV antigen to a degree equivalent to that of its homologous antigen (Table 1).

Immunohistochemistry of naturally infected eiders. To determine if WFBV antigen colocalized with observed microscopic lesions, we tested common eiders by IHC that were showing clinical signs of disease prior to death and from which WFBV was subsequently isolated. As shown in Fig. 2C, WFBV antigen was detected in areas of hepatocellular necrosis, demonstrating that WFBV was responsible (at least in part) for the observed microscopic lesions present in moribund birds.

Genomic sequencing. WFBV isolate 10-280-G, recovered from the liver of a common eider in 2010, was used as the template for genomic sequencing. The resulting genome is believed to be composed of at least seven RNA segments ranging from approximately 0.5 to 2.4 kb in length (Fig. 4). The consensus sequences of the conserved terminal ends of the genome were 5′-AGCAAUC ACAA and UUGUUAUUGCU-3′, nearly identical to those observed in QRFV (23), and exhibited perfect inverse complementarity other than position 7 from each end (underlined) (49). Whether other proteins are expressed from the WFBV genome (e.g., by splicing or in overlapping open reading frames [ORFs]) in addition to the seven proteins listed below is currently unknown.

Segments 1 to 3: polymerase proteins (PA, PB1, PB2). The three largest RNA segments of the WFBV genome are similar in size (ranging from 2,403 to 2,427 nucleotides [nt] in length) and encode the proteins comprising the polymerase complex, as based upon their detectable identity to the cognate influenza virus proteins. Segment 1 is 2,427 nt long and encodes PB2 (90.9 kDa); segment 2 is 2,414 nt long and encodes PB1 (87.1 kDa); and segment 3 is 2,403 nt long and encodes PA (90.7 kDa). A number of consensus motifs in the PB1 of influenza viruses (I to IV) (50) were also present in the WFBV PB1, including the characteristic SDD motif involved in polymerization activity (51).

Segment 4: nucleoprotein. Segment 4 is 1,691 nt long and encodes a 537-amino-acid (aa), 60.4-kDa product believed to be the putative nucleoprotein (NP). The NP of WFBV shares a 45.8% to 47.4% amino acid identity to the "hypothetical proteins" of QRFV and TLKV (GenBank accession numbers JN412853 and AEW22798, respectively), although it does not align with other orthomyxoviruses by standard protein alignment searches (i.e., BLAST, HHBlits, HHpred). However, protein BLAST searches with a virus organism query (using the UniProtKB/Swiss-Prot or

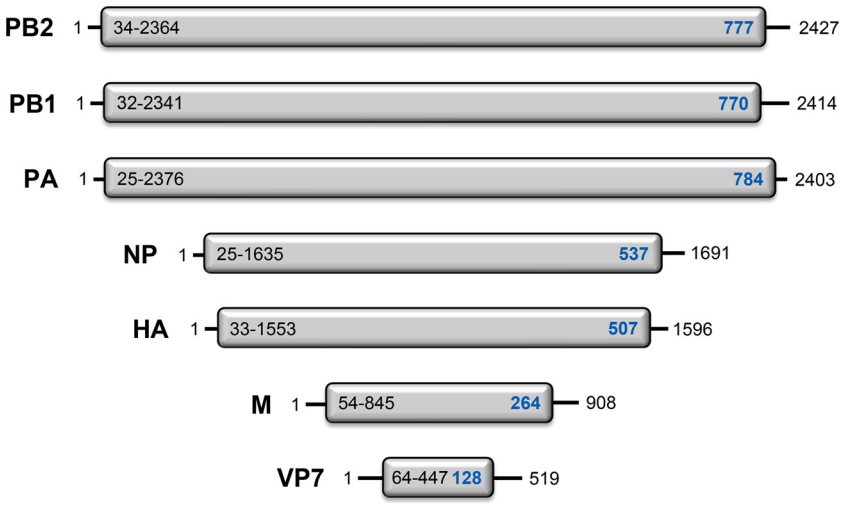

FIG 4 Segmental configuration of the WFBV genome and identification of a new orthomyxovirus gene (VP7). All seven identified RNA segments of the WFBV genome are shown in positive-sense orientation in decreasing size from top to bottom. For each segment, the 5′ and 3′ terminal noncoding regions (NCRs) are shown as thin black lines, and each open reading frame (ORF) is shown as a thick gray bar. The nucleotides encompassing the ORF of each gene are shown (in black) on the left side of each gray bar, while the size of the protein product (in amino acids) produced from the ORF is shown (in blue) on the right. The total length of each RNA segment (NCRs and ORF) is shown on the very far right. Note that the smallest segment (segment 7) is 519 nt long and encodes a previously undescribed protein of unknown function (tentatively designated VP7). The complete genome of WFBV has been deposited in GenBank under the accession numbers KM114304 to KM114310.

nonredundant databases), in addition to structural alignments generated in Phyre2, demonstrated identity to a number of orthomyxovirus NPs, including those of THOV, Jos virus (JOSV), FLUBV, and FLUCV (not shown), strongly suggesting that segment 4 in WFBV indeed encodes the NP. It is also of interest that the closest match to the WFBV NP after the QRFV and TLKV hypothetical proteins by standard protein BLAST analysis is the hypothetical protein IscW_ISCW004769, identified in the black-legged tick (*Ixodes scapularis*) (GenBank accession no. XP_002433660). The significance of this protein homology is speculative but clearly warrants further inquiry.

Segment 5: hemagglutinin protein. Segment 5 is 1,596 nt long and encodes the predicted 507-aa, 57.8-kDa HA protein. The WFBV HA contains a predicted signal peptide (residues 1 to 17), a large ectodomain (residues 18 to 480), followed by a C-terminal transmembrane domain (residues 481 to 505) and a very short cytoplasmic tail (residues 506 to 507). The WFBV HA, like the surface glycoproteins of other quaranjaviruses and thogotoviruses, bears sequence and structural similarities to the gp64 protein of group I alphabaculoviruses (15) (see "Molecular modeling of the WFBV HA protein").

Segment 6: matrix protein. Segment 6 is 908 nt long and encodes a 264-aa, 29.7-kDa product believed to be the putative matrix (M) protein. The M protein of WFBV shares a 31.4% to 33.0% amino acid identity to the unknown and hypothetical protein gene segments of QRFV and TLKV, respectively (GenBank accession numbers ACY56280 and AFN73051). Remarkably, however, the M protein of WFBV shares an 82.0% nucleotide and 89.0% amino acid identity to the putative M protein of Cygnet River virus (CyRV) (see Discussion for details) (34). Although no sequence similarity could be detected between the tentative M proteins of quaranjaviruses and other orthomyxoviruses, the predicted size, molecular mass, and isoelectric point of the putative WFBV M protein (264 aa, 29.7 kDa, 8.9), compatible to those of FLUAV M1 (252 aa, 27.9 kDa, 9.3), in addition to motifs such as a multibasic sequence ^{217}-RKLR-^{220} similar to the ^{101}-RKLKR-^{105} nuclear localization signal of FLUAV M1 (52), suggest that segment 6 of WFBV encodes the M protein. Additionally, a protein band approximately 30 kDa in size was abundantly present in purified virions and was demonstrated to be the putative M by peptide sequencing (see "Structural protein analysis"), suggesting that this protein is a high-copy-number component of the virion, indicative of a matrix-like protein.

Segment 7: unknown protein (VP7). Segment 7 is 519 nt long and encodes a previously undescribed protein of unknown function (tentatively named viral protein 7 [VP7]) that is 128 aa in length with an estimated molecular mass of 14.3 kDa. Nucleotide or protein BLAST, PatternSearch, HHblits, HHpred, HHsenser, and Phyre2 searches of VP7 did not reveal significant sequence or structural homology to any viral or cellular protein. To investigate this apparent lack of homology further, we attempted to identify any possible motifs or sequence/structural conservation in VP7 versus other proteins through additional analyses. Manual alignments to other orthomyxovirus proteins identified some similarities between VP7 and FLUAV nonstructural protein 2 (NS2). Both proteins are similarly sized, being 121 to 128 amino acids in length and 14.30 to 14.38 kDa. Common short sequences of identity between the two proteins included the first four amino acids (^{1}-MDPN-^{4}) and the presence of a highly conserved serine-rich motif (^{23}-SSS-^{25} in FLUAV; ^{97}-SSS-^{99} in WFBV) demonstrated to be involved in phosphorylation of FLUAV NS2 (53). Analysis for leucine-rich areas in VP7 identified a region predicted to be part of a nuclear export signal (NES) (^{28}-MALSGDLLRLL-^{38}; underlined residues are hydrophobic amino acids). Although this predicted NES does not strictly adhere to the common consensus sequence of L-X(2,3)-[LIVFM]-X(2,3)-L-X-[LI], only 36% of high-quality NESs have previously been shown to fit this prediction (54). Additionally, motif prediction analysis using a Prosite pattern scan demonstrated a strong match of the N-terminal region encompassing ^{14}-RCSTLNWAQSMHQIMALSGDLLR-^{36} (which includes part of the predicted NES) to the ribosomal protein S14 (rpS14) signature motif [RP]-X(0,1)-C-X(11,12)-[LIVFM]-{L}-[LIVFM]-[SC]-[RG]-X-{D}-{PK}-[RN]. rpS14 is a component of the 40S subunit that, in addition to its role in ribosomal assembly and function (55, 56), has been shown to be involved in p53 activation (57) and c-Myc inhibition (58). Although it is currently uncertain if any of these predicted motifs are indeed indicative of true functionality, of 1,004 UniProtKB/Swiss-Prot sequences known to belong to the rpS14 class, 792 were detected using the Prosite pattern scan (78.9% positive), 212 were undetected (21.1% false negatives), with only 33 false positives (of 542,502 entries), resulting in a precision rate [true positives/(true positives + false positives)] of 95.9% (http://prosite.expasy.org/PDOC00456).

Structural protein analysis. SDS-PAGE analysis of purified virions demonstrated a number of discernible bands that, based on their approximate molecular masses, were believed to represent M, NP, and HA and possibly the polymerase proteins (Fig. 5). To further clarify these tentative designations, each band was excised from a SYPRO ruby-stained gel and analyzed by nano HPLC-MS/MS. Viral and cellular proteins identified from each of the gel-excised bands are shown in Fig. S1 in the supplemental material. Mass spectrometric analysis demonstrated that the putative M, HA, and NP migrated close to their approximate predicted molecular masses, with the NP (predicted, 60.4 kDa) migrating just below the HA protein (predicted, 57.8 kDa) (Fig. 5). PA, PB1, and PB2 were also detected in purified virions (second asterisk from the top in Fig. 5), although they were found at much lower levels than M, NP, and HA (possibly owing to their low concentration within particles relative to other structural proteins) and not as discrete bands (expected molecular masses of 87.1 to 90.9 kDa). The majority protein in the upper discernible high-molecular-mass bands (shown as asterisks in Fig. 5) corresponded to syndecan 4, a small membrane-associated heparan sulfate proteoglycan that can form large SDS-resistant oligomers (59). Interestingly, interactions of syndecan 4 with virus-associated apolipoprotein E has been shown to mediate *Hepatitis C virus* entry into liver cells (60). Although a distinct low-molecular-mass band (~15 kDa) suggestive of VP7 was not readily detected by our methods (suggesting it may be a nonstructural protein), we identified peptides corresponding to VP7 within virions (see Fig. S1 in the supplemental material), definitively showing it is being produced during infection. Additionally, a single ribosomal protein, rpS4X (61), was found within WFBV particles (see Fig. S1). Whether the incorporation of VP7 and these cellular proteins into virions is a random or selective process is currently unknown.

Molecular modeling of the WFBV HA protein. The predicted three-dimensional structure of the WFBV HA generated in Phyre2 using the AcMNPV gp64 protein (PDB 3DUZ) as the template is shown in Fig. 6A. The probability (confidence) that the

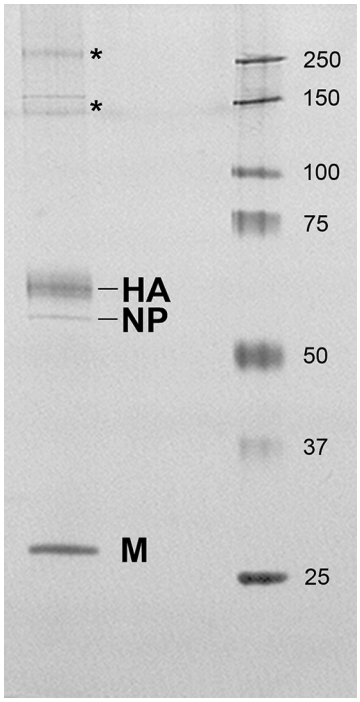

FIG 5 Structural protein analysis of WFBV. Purified virions were analyzed by SDS-PAGE followed by nanoscale high-performance liquid chromatography coupled to tandem mass spectrometry (nano HPLC-MS/MS). All discrete bands in the gel were excised and subjected to tryptic digestion, and peptides were identified by nano HPLC-MS/MS (see Fig. S1 in the supplemental material for peptide analysis). The molecular masses (kDa) of the individual proteins in the ladder (right) are indicated for cross-reference. Note that the putative M protein (predicted to be 29.7 kDa) is abundantly present in virions. Although peptides corresponding to PA, PB1, and PB2 were detected in visible bands (lower asterisk), discrete bands for these polymerase proteins were not visible, possibly owing to their low abundance within virus particles relative to other structural proteins. The majority protein present in the high-molecular-mass bands (two asterisks) was syndecan 4, a cellular transmembrane proteoglycan.

match between WFBV HA and AcMNPV gp64 was a true homology was 100%, with 84% of the protein (425 residues) modeled at >90% confidence. Eighty residues of the WFBV HA were modeled *ab initio*, as these regions were either missing (i.e., signal peptide and C-terminal transmembrane and cytoplasmic domains) or disordered in the cognate gp64 ectodomain structure (17); thus, the accuracy of these inferred structures in the WFBV HA (shown in black in Fig. 6A) is not reliable.

Although the AcMNPV gp64 and WFBV HA share only 21.8% amino acid identity, the overall structure of the two glycoproteins was well conserved, allowing for the prediction of putative domains and motifs in the HA structure of WFBV. Notably, domain III of the two receptors, which contains a triple-stranded α-helical coiled coil that forms the long central stalk in the trimer (17), shared similar structures (Fig. 6A), albeit with little sequence conservation in the coil itself (11.9% amino acid identity) (see Fig. S2 in the supplemental material). Overall, the model of the WFBV HA showed a high level of conservation in domains Ia, Ib, III, IV, and V. Structurally, the most divergent domain between the two proteins was domain II, which forms two four-stranded antiparallel β-sheets in AcMNPV (Fig. 6A) (17). Interestingly, two disulfide bridges (V and IV) stabilize this domain in AcMNPV and the thogotoviruses (THOV, DHOV) but not in WFBV, as it does not contain the 6th disulfide bridge (see Fig. S2).

As the WFBV HA and AcMNPV gp64 showed remarkable structural conservation, we further investigated whether the residues or overall topology of the terminal fusion loops that have been implicated in AcMNPV membrane fusion and receptor binding activity were also conserved in WFBV. Previously, it has been demonstrated that substitutions at L82, F153, and A154 in AcMNPV gp64 could abolish fusion and that mutating F153 (along with H156) could also decrease virus binding, suggesting that both fusion activity and receptor binding may map to the same area of gp64 (17, 62). Further analysis of AcMNPV gp64 indicated two regions of the fusion loops (residues Y75 to T86 in loop 1 and N149 to H156 in loop 2) were critical for fusion activity, with three histidines in loop 2 (H152, H155, and H156) important for pore expansion (22, 63). Comparison of the WFBV fusion loops to that of AcMNPV demonstrated that loop 1 was well conserved (^{75}-YCYSGGAVDPNT-^{86}; underlined residues are identical, with AcMNPV numbering shown), with more variability in loop 2 (^{149}-EYYYLFPHH-^{156}), although both F153 and H156 (involved in membrane binding) were conserved between the two viruses (Fig. 6B). Indeed, these two residues are conserved across all quaranjaviruses, thogotoviruses, and baculoviruses analyzed (WFBV, QRFV, THOV, DHOV, AcMNPV) (see Fig. S2), suggesting that host cell binding may proceed in a similar fashion.

Fusion assay. WFBV-infected Vero E6 cells that were transiently treated at a low pH demonstrated fusogenic activity, as exemplified by the formation of various-sized syncytia, followed by their subsequent detachment from the monolayer (Fig. 6D). To determine if the HA was solely responsible for the observed fusogenic activity of WFBV, we subcloned the HA of the prototype WFBV 10-280-G into pcDNA 3.1(−) and transfected Vero E6 cells. Expression of HA in transfected cells was verified by Western blotting using WFBV MHIAF (not shown). As with live virus, fusion in cells expressing HA alone was characterized by the formation of numerous syncytia (Fig. 6G and H) and was evident within hours of low-pH treatment, demonstrating that the HA (in the absence of other WFBV proteins) causes fusion similar to that observed with live WFBV and also compatible with cell-to-cell fusion observed during transient expression of AcMNPV gp64 (17, 63).

Experimental host range. WFBV was shown to have a broad host range *in vitro*. All avian (Pekin duck, Japanese quail) and mammalian (human, African green monkey, rhesus macaque, Mexican free-tailed bat, Virginia opossum, American mink, cattle) cell lines tested were susceptible to infection and supported replication to various degrees (maximum titers of $10^{6.15}$ to $10^{8.02}$ PFU/ml). However, WFBV did not replicate in C6/36 cells derived from *Aedes albopictus*, similar to results reported for QFRV and JAV (23, 64) as well as CyRV (34), demonstrating an *in vitro* host range barrier for Asian tiger mosquito cells in all tested quaranjaviruses.

Phylogenetic analysis. Our phylogenetic analysis of 378 conserved amino acid residues within PB1 clearly showed that WFBV is a newly described member of the genus *Quaranjavirus*, forming a monophyletic group with JAV, QRFV, and TLKV (Fig. 7A). However, phylogenetic relationships within this genus are not clear and only offer tentative support for a clustering of WFBV and JAV (60% bootstrap support), with 30% amino acid divergence. A phylogenetic analysis on a longer (766-aa residue) PB1 alignment of the four quaranjaviruses taken in isolation failed to

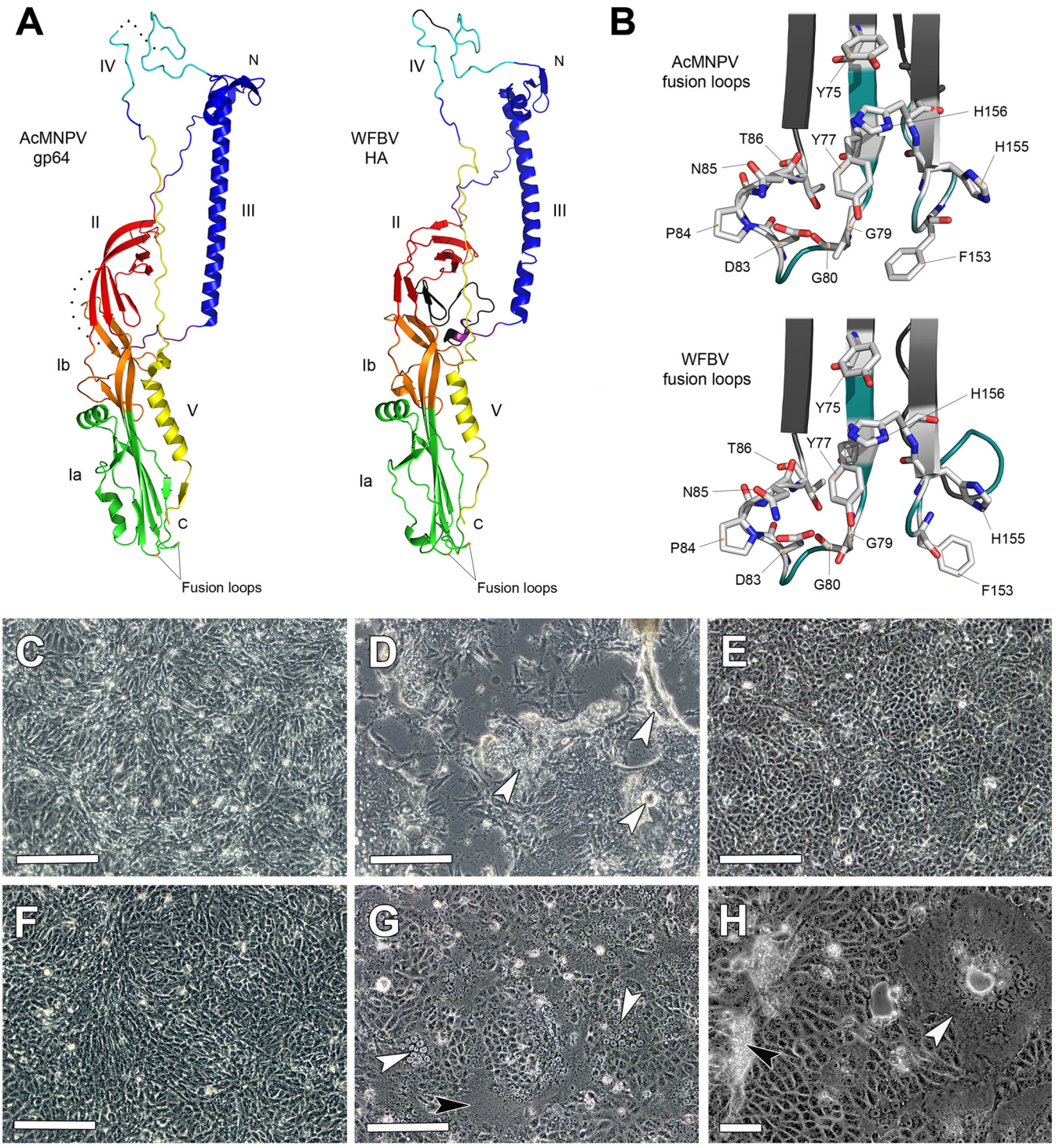

FIG 6 Fusion activity of the WFBV hemagglutinin (HA) protein and the predicted molecular model of the HA monomer showing its structural relationship to the postfusion conformation of group I alphabaculovirus gp64. (A) The WFBV HA protein was modeled using the *Autographa californica nucleopolyhedrovirus* (AcMNPV) gp64 protein as the template (PDB 3DUZ). The highlighted domains of the WFBV HA (I to V) are based on the homologous domains of the baculovirus gp64. Disordered regions of the AcMNPV gp64 (denoted as dots) (17) are shown in black in WFBV. Note the location of the fusion loops in domain Ia and the highlighted N and C termini. (B) Comparison of the fusion loops of AcMNPV gp64 and WFBV HA. Residues Y75 to T86 in loop 1 and N149 to H156 in loop 2 are critical for fusion activity and receptor binding (22), with three histidines in loop 2 (H152, H155, and H156) important for pore expansion (63). Conserved residues are highlighted by stick representations, with differences between the two viruses shown in marine. Residues outside the Y75-T86 and N149-H156 regions are shown in dark gray. (C to H) pH-dependent cell-to-cell fusion in virus-infected and HA-transfected cells. WFBV-infected (10-280-G) Vero cells (C) were incubated in MEM (pH 4.0) for 10 min and then returned to physiological pH (pH 7.4) (D). Note the formation of various-sized syncytia (arrowheads) in WFBV-infected cells 24 h after low-pH treatment, as shown in panel D. In transfection experiments, neither Vero cells transfected with empty vector and low-pH-treated (E) or HA-transfected cells at physiological pH (F) demonstrated cell-to-cell fusion. However, discrete syncytium formation was evident within 4 h of low-pH treatment in HA-transfected cells (G), as demonstrated by the congregation of nuclei (white arrowheads) and development of large expanses of cytoplasm (black arrowhead). A closeup photo of HA-transfected cells 24 h after low-pH treatment (H) clearly demonstrated large classical multinucleated cells (white arrowhead), along with late-stage detachment of syncytia (black arrowhead). Scale bars = 200 μm.

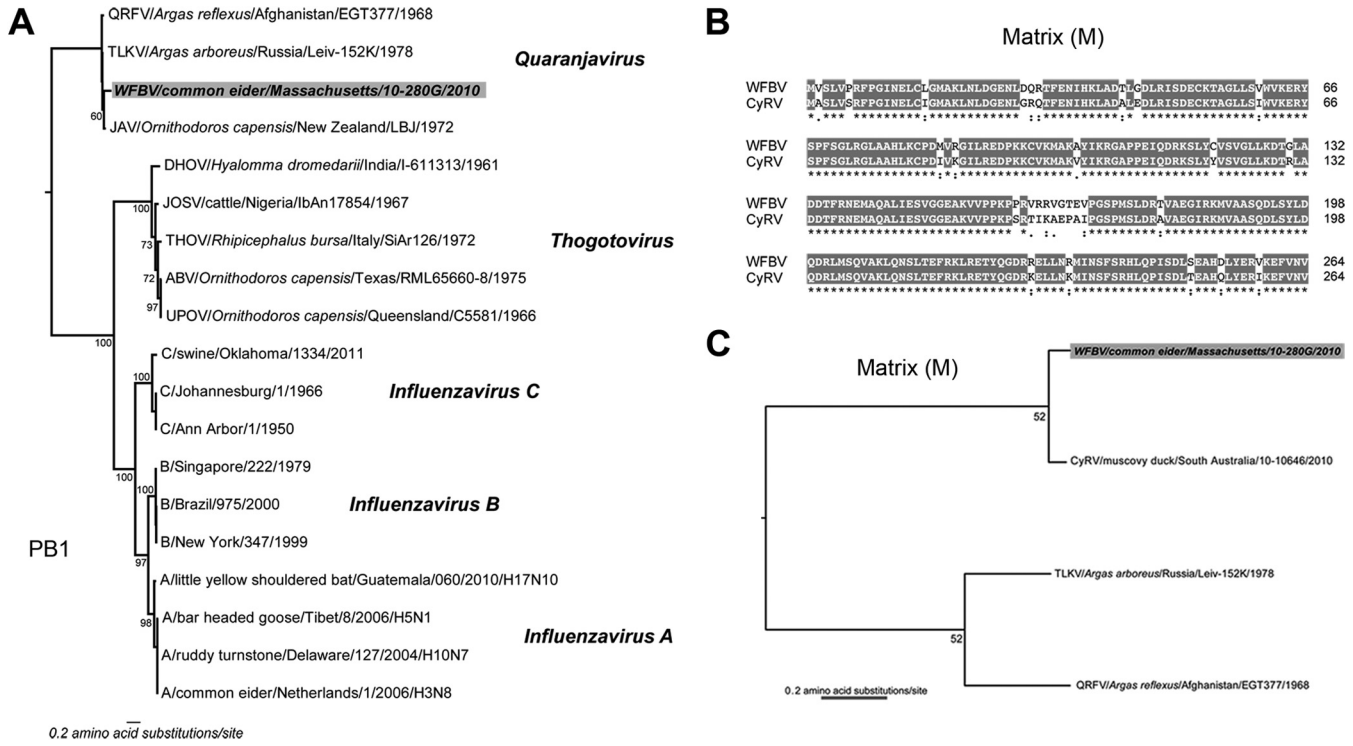

FIG 7 Evolutionary relationships of WFBV and other orthomyxoviruses. (A) Phylogeny based on the PB1 amino acid sequences of representative members of five genera of *Orthomyxoviridae* is shown. The tree is drawn to a scale of amino acid substitutions per site (with all ambiguously aligned positions removed), and all bootstrap values of >70% are shown, along with the bootstrap value relating to WFBV. The tree is midpoint rooted for purposes of clarity only. Viruses are shown as designated or proposed ICTV abbreviation/host/location/strain/year. Viruses (and their GenBank accession numbers) are as follows (note only ICTV-approved species are italicized): ABV, Aransas Bay virus RRML65660-8 (KC506163); DHOV, *Dhori virus* I-611313 (P27153); FLUAV, *Influenza A virus* Netherlands/1 (ACR58714), Tibet/8 (ADG59444), Guatemala/060 (AFC35436), and Delaware/127 (ACZ45637); FLUBV, *Influenza B virus* Singapore/222 (AAF06873), Oklahoma/347 (ACN32565), and Brazil/975 (ABL84349); FLUCV, *Influenza C virus* Ann Arbor/1 (YP_089653), Johannesburg/1 (Q9IMP4), and Oklahoma/1334 (AFJ19019); JAV, *Johnston Atoll virus* LBJ (ACY56284); JOSV, Jos virus IbAn17854 (AED98371); QRFV, *Quaranfil virus* EGT377 (ACY56282); THOV, *Thogoto virus* SiAr126 (YP_145794); TLKV, Tyulek virus Leiv152 (AFN73049); UPOV, Upolu virus C5581 (KC506157); and WFBV, Wellfleet Bay virus 10-280-G (KM114305). (B) Amino acid alignment of the matrix (M) proteins of WFBV and Cygnet River virus (CyRV), demonstrating the high identity between the two viruses. Viruses used in the alignment were WFBV 10-280-G (KM114309) and CyRV 10-10646 (AFB81541). (C) Phylogeny based on M amino acid sequences of available quaranjaviruses. The tree is drawn to a scale of amino acid substitutions per site and is midpoint rooted for purposes of clarity only. Viruses are shown as designated or proposed ICTV abbreviation/host/location/strain/year. Viruses (and their GenBank accessions) are as follows: CyRV 10-10646 (AFB81541), QRFV EGT377 (ACY56280), TLKV Leiv152 (AFN73051), and WFBV 10-280-G (KM114309).

improve resolution, with all bootstrap values of <50%. Additionally, analysis of the putative M proteins for available quaranjaviruses indicated that WFBV and CyRV clustered together, as did QRFV and TLKV (Fig. 7C). Although the putative M proteins of WFBV and CyRV share 89.0% amino acid identity (Fig. 7B) and are clearly closely related, bootstrap levels were low (Fig. 7C), most likely due to the short and limited number of sequences in the data set. Overall, it appears that the 12 orthomyxoviruses confirmed or suspected to be tick-borne can most likely be grouped into two defined genera: (i) *Quaranjavirus*, tentatively encompassing QRFV, JAV, LKCV, TLKV, CyRV, and WFBV, and (ii) *Thogotovirus*, tentatively encompassing THOV, DHOV (including Batken, a variant of DHOV), JOSV, Upolu virus (UPOV), Aransas Bay virus (ABV), and Araguari virus (ARAV) (23, 34, 65–69).

DISCUSSION

This is the first report and identification of a novel orthomyxovirus (Wellfleet Bay virus [WFBV]) that has been associated with large-scale die-offs of common eiders that have occurred cyclically along the coast of Cape Cod, MA, for at least the past 15 years. In general, most bird-associated orthomyxoviruses, such as FLUAV, along with the historically isolated but recently characterized QRFV and JAV (23), appear to predominately cause subclinical infections in their normal avian hosts (5, 30, 33). In contrast, WFBV may cause fatal infections in wild birds. However, the nature of the observed pathogenicity is ambiguous, as it is presently unclear whether WFBV (i) is normally a mild pathogen that periodically causes low-level morbidity and isolated mortality events that generally go unrecognized but can result in epidemic disease when exacerbated by predisposing environmental conditions (e.g., nutritional stress) or underlying coinfections (e.g., acanthocephalans), (ii) is an endemic and benign virus of eiders that recently underwent genetic change that increased its virulence, or (iii) recently jumped into common eiders from another yet-unknown host, thus resulting in the apparently recent observation of severe clinical disease (70). Although the natural host range of WFBV is currently unknown, as it has not yet been isolated from any species other than common eiders, the virus replicates in a variety of avian and mammalian cell lines, suggesting it may be able to infect a diverse range of hosts in nature.

Genomic analysis of WFBV indicated that in addition to the six prototypical negative-sense, single-stranded RNA segments encoding the standard structural proteins (HA, M, NP, PA, PB1, PB2) reported for QFRV (4, 23) and TLKV (46), WFBV contains a previously unknown segment. This newly discovered segment (segment 7) was the shortest RNA molecule identified in the genome, being only 519 nucleotides long and encoding a 128-amino-acid 14.3-kDa protein that we tentatively designated VP7 (Fig. 4). Although no strongly supported homology could be detected to any known viral or cellular proteins, motif predictions indicated that VP7 contained a conserved 23-amino-acid domain found in eukaryotic ribosomal protein S14 (rpS14), a member of the 40S subunit and S11P family of ribosomal proteins (71, 72). Although the role of this WFBV protein in the viral life cycle is speculative until protein expression and functional studies are performed, its compact size coupled with the identification of the six major conserved orthomyxovirus structural proteins (HA, M, NP, PA, PB1, PB2) suggest VP7 may be a nonstructural protein involved in some ancillary stage(s) of viral infection (e.g., enhancing translation of viral mRNAs, nuclear transport [73, 74]). Interestingly, ribosomal protein S4, another 40S subunit member that (like rpS14) is part of the small-subunit processome (75) and is unique among ribosomal proteins in that it has serine protease activity (76), was found within WFBV particles; whether this or other cellular proteins found within virions (see Fig. S1 in the supplemental material) are selectively or randomly incorporated remains to be determined. Additionally, the identification of segment 7 (if present) in other quaranjaviruses (or possibly in thogotoviruses other than THOV) will aid in identifying conserved motifs in the protein that may be essential for function (51, 77).

The apparent host of WFBV, the common eider, is a sea duck that aggregates in large nesting colonies (which can number >20,000 birds) (2) and thus fits the expected profile of a prototypical vertebrate host for a quaranjavirus (i.e., colonial, densely nesting aquatic bird species). Like other quaranjaviruses, WFBV encodes a glycoprotein receptor (HA) that is similar to the gp64 protein of certain alphabaculoviruses (15, 23). Although the two proteins shared limited amino acid identity, the overall predicted structures between the two proteins were remarkably similar (Fig. 6A). Additionally, cell-to-cell fusion could be induced in WFBV-infected (Fig. 6D) or HA-transfected cells (Fig. 6G to H) by transition to low pH, suggesting the pH-dependent fusogenic activity of gp64 (63) is conserved in the HA of WFBV and that the WFBV HA is likely a new member of the class III family of fusion proteins (17). Although the nature of the transmission mechanism of WFBV has yet to be identified, it is most likely that either soft or hard ticks are the primary vectors of the virus. Common eiders are native to the northern latitudes of North America, Europe, and the Russian Far East (2), where hard ixodid ticks are found almost exclusively (32). The near circumpolar distribution of the common eider suggests that WFBV is either aberrantly vectored (in relation to other quaranjaviruses) by a hard tick species or vectored by a soft tick clandestinely inhabiting Massachusetts and/or other northern regions. However, since QRFV has also been recovered from hard ticks (27), combined with the lack of any records of sea bird-associated soft ticks being present in New England and Canada (78), this suggests that WFBV may be transmitted in nature by a hard tick species such as *Ixodes uriae*, which is a common parasite of colonial nesting seabirds (including common eiders) in the northeastern United States (79) and a demonstrated vector of numerous arboviruses (80–82). However, alternative (or additional) means of transmission, such as aerosol, fecal-oral, water-based, or other arthropod-borne (e.g., insect) routes, cannot be ruled out and should be investigated. Additionally, how (or whether) this yet-to-be-identified transmission cycle plays a role in the temporal (cyclic) and spatial (Cape Cod region) observance of disease is unknown. As the annual movement patterns, body composition, ectoparasite diversity, and population demographics of common eiders have begun to be monitored closely over the past few years in recognition of the die-offs, such ecological studies should provide additional insight into WFBV epidemiology, thus potentially identifying ways in which population impacts due to disease may be mitigated in the future.

The genetic distance between WFBV and influenza viruses is substantial, with the viruses sharing detectable amino acid identity in partial sequences of PA, PB1, PB2, and NP only. In relation to the currently classified and tentative quaranjaviruses for which complete PB1 sequences are available (QRFV, JAV, TLKV), WFBV clustered with JAV in the PB1 phylogeny (Fig. 7A), although with weak support. Concordantly, our antigenic analysis of WFBV against QRFV, JAV, TLKV, and LKCV, along with all other known tick-borne orthomyxoviruses (i.e., thogotoviruses), did not demonstrate any detectable cross-reactions by complement fixation testing (Table 1). Additionally, as expected, antigenic cross-reactions between WFBV and FLUAV were not observed (not shown). However, the most intriguing finding was that WFBV was closely related to, and potentially appears to share common host and pathological properties with, the newly identified Cygnet River virus (CyRV), a novel orthomyxovirus isolated from an outbreak of clinical disease in captive Muscovy ducks (*Cairina moschata*) along the Cygnet River in Kangaroo Island, South Australia (34). Similar to the cyclic outbreaks involving WFBV in Cape Cod, the epizootic of CyRV was characterized by premonitory clinical signs such as lethargy and diarrhea, prominent histopathological lesions in the liver, and large-scale mortality in ducks (34). The apparent similarities between the two viruses were further extended, as comparisons of the complete matrix (M) proteins between WFBV and CyRV demonstrated an 89.0% amino acid identity (Fig. 7B). Unfortunately, other than M, no other sequences of CyRV are currently available in public databases for comparison. In addition, the two viruses were indistinguishable by complement fixation tests (Table 1), providing further evidence that WFBV and CyRV may be geographically separated strains of the same virus (or at least very closely related viruses) that are apparently circulating at opposite ends of the globe. If this is indeed the case, one tentative mechanism for their divergence is through the transoceanic transport of an infected tick on a migrating pelagic bird species and/or through a prolonged viremia in such a host. For example, *Ixodes uriae*, a hard tick species that is present in both southern and northern circumpolar regions where the two outbreaks have occurred (32), has previously been recovered from pelagic birds that undergo transoceanic migrations between Australasia and North America (83, 84). Similarly, JAV was first isolated in Johnston Atoll in the north Pacific (25) and later from seabird colonies in Hawaii (28), Australia (29), and New Zealand (30), indicating movement of quaranjaviruses across large expanses of the Pacific Ocean. Nevertheless, until full genome comparisons between WFBV and CyRV are performed, the exact nature of their relationship will remain unknown.

Although WFBV has been isolated from clinically sick birds in multiple outbreak years and antigen has been detected in pathological lesions (Fig. 2C), whether it is an opportunistic pathogen that becomes virulent only in concert with underlying conditions (e.g., malnutrition) or coinfections is uncertain but is currently being assessed in experimental trials. As the recovery of *Salmonella* from dead Muscovy ducks during the CyRV outbreak of 2010 suggests that clinical disease in virus-infected birds may be dependent upon the additive or synergistic effects of concurrent infections (34), investigation into the detection of other pathogens in association with WFBV infection, such as through metagenomic analysis of eider tissues, will also be a focus of future research. The observed epidemics of disease involving a novel orthomyxovirus in the United States warrants further study not only to better understand the underlying causes of these outbreaks but to also clarify the evolution, epidemiology, and ecology of these newly emerging orthomyxoviruses.

ACKNOWLEDGMENTS

Funding for this research was provided by United States Department of the Interior (USDI) Cooperative Agreement F12AP0122 to A.B.A. Additional support was provided by the wildlife management agencies of the SCWDS member states through the Federal Aid to Wildlife Restoration Act (50 Stat.917) and by USDI Cooperative Agreement G11AC20003. E.C.H. was supported by a National Health and Medical Research Council Australia Fellowship. A.B.A. is additionally supported through an NRSA postdoctoral fellowship (F32AI100545) from the National Institute of Allergy and Infectious Diseases, National Institutes of Health.

We thank Gary Blissard at the Cornell Boyce Thompson Institute, Peter Schweitzer, Wei Chen, and Sheng Zhang of the Cornell University Institute of Biotechnology, and Steven Kubiski at UC Davis. We also thank the staff of the Cape Cod National Seashore, particularly Robert Cook and Mary Hake, and the volunteers at the Seabird Ecological Assessment Network (SEANET; Cummings School of Veterinary Medicine, Tufts University) for their assistance in monitoring for and detecting die-offs and assisting with field collections and logistics.

Use of products or trade names is not an endorsement by the United States government.

REFERENCES

1. **Clark GM, O'Meara D, Van Weelden JW.** 1958. An epizootic among eider ducks involving an acanthocephalid worm. J Wildlife Manage **22:**204–205. http://dx.doi.org/10.2307/3797332.
2. **Goudie RI, Robertson GJ, Reed A.** 2000. Common eider (Somateria mollissima). *In* Poole AF, Gill FB (ed), The birds of North America, no. 177. The Academy of Natural Sciences, Washington, DC.
3. **Hario M, Lehtonen JT, Hollmén T.** 1995. Role, if any, of the acanthocephalan worm *Polymorphus minutus* in common eider mortality. Suomen Riista **41:**21–26.
4. **McCauley JW, Hongo S, Kaverin NV, Kochs G, Lamb RA, Matrosovich MN, Perez DR, Palese P, Presti RM, Rimstad E, Smith GJD.** 2011. Family Orthomyxoviridae, p 749–761. *In* King AMQ, Adams MJ, Carstens EB, Lefkowitz EJ (ed), Virus taxonomy: ninth report of the International Committee on Taxonomy of Viruses. Elsevier Academic Press, San Diego, CA.
5. **Webster RG, Bean WJ, Gorman OT, Chambers TM, Kawaoka Y.** 1992. Evolution and ecology of influenza A viruses. Microbiol Rev **56:**152–179.
6. **Brankston G, Gitterman L, Hirji Z, Lemieux C, Gardam M.** 2007. Transmission of influenza A in human beings. Lancet Infect Dis **7:**257–265. http://dx.doi.org/10.1016/S1473-3099(07)70029-4.
7. **Imai M, Herfst S, Sorrell EM, Schrauwen EJ, Linster M, De Graaf M, Fouchier RA, Kawaoka Y.** 2013. Transmission of influenza A/H5N1 viruses in mammals. Virus Res **178:**15–20. http://dx.doi.org/10.1016/j.virusres.2013.07.017.
8. **Wright PF, Neumann G, Kawaoka Y.** 2013. Orthomyxoviruses, p 1186–1243. *In* Knipe DM, Howley PM (ed), Fields virology, 6th ed. Lippincott Williams and Wilkins, Philadelphia, PA.
9. **Nylund A, Hovland T, Hodneland K, Nilsen F, Løvik P.** 1994. Mechanisms for transmission of infectious salmon anaemia (ISA). Dis Aquat Org **19:**95–100. http://dx.doi.org/10.3354/dao019095.
10. **Marshall SH, Ramírez R, Labra A, Carmona M, Muñoz C.** 2014. Bona fide evidence for natural vertical transmission of infectious salmon anemia virus (ISAV) in freshwater brood stocks of farmed Atlantic salmon (Salmo salar) in Southern Chile. J Virol **88:**6012–6018. http://dx.doi.org/10.1128/JVI.03670-13.
11. **Haig DA, Woodall JP, Danskin D.** 1965. Thogoto virus: a hitherto undescribed agent isolated from ticks in Kenya. J Gen Microbiol **38:**389–394. http://dx.doi.org/10.1099/00221287-38-3-389.
12. **Anderson CR, Casals J.** 1973. *Dhori virus*, a new agent isolated from *Hyalomma dromedarii* in India. Indian J Med Res **61:**1416–1420.
13. **Jones LD, Davies CR, Steele GM, Nuttall PA.** 1987. A novel mode of arbovirus transmission involving a nonviremic host. Science **237:**775–777. http://dx.doi.org/10.1126/science.3616608.
14. **Hubálek Z, Rudolf I.** 2012. Tick-borne viruses in Europe. Parasitol Res **111:**9–36. http://dx.doi.org/10.1007/s00436-012-2910-1.
15. **Morse MA, Marriott AC, Nuttall PA.** 1992. The glycoprotein of Thogoto virus (a tick-borne orthomyxo-like virus) is related to the baculovirus glycoprotein gp64. Virology **186:**640–646. http://dx.doi.org/10.1016/0042-6822(92)90030-S.
16. **Monsma SA, Oomens AG, Blissard GW.** 1996. The gp64 envelope fusion protein is an essential baculovirus protein required for cell-to-cell transmission of infection. J Virol **70:**4607–4616.
17. **Kadlec J, Loureiro S, Abrescia NG, Stuart DI, Jones IM.** 2008. The postfusion structure of baculovirus gp64 supports a unified view of viral fusion machines. Nat Struct Mol Biol **15:**1024–1030. http://dx.doi.org/10.1038/nsmb.1484.
18. **Friesen PD.** 2013. Insect viruses, p 2326–2354. *In* Knipe DM, Howley PM (ed), Fields virology, 6th ed. Lippincott Williams and Wilkins, Philadelphia, PA.
19. **Afonso CL, Tulman ER, Lu Z, Balinsky CA, Moser BA, Becnel JJ, Rock DL, Kutish GF.** 2001. Genome sequence of a baculovirus pathogenic for Culex nigripalpus. J Virol **75:**11157–11165. http://dx.doi.org/10.1128/JVI.75.22.11157-11165.2001.
20. **Arif B, Escasa S, Pavlik L.** 2011. Biology and genomics of viruses within the genus *Gammabaculovirus*. Viruses **3:**2214–2222. http://dx.doi.org/10.3390/v3112214.
21. **Nuttall PA, Morse MA, Jones LD, Portela A.** 1995. Adaptation of members of the Orthomyxoviridae family to transmission by ticks, p 416–425. *In* Gibbs AJ, Calisher CH, Garcia-Arenal F (ed), Molecular basis of virus evolution. Cambridge University Press, Cambridge, United Kingdom.
22. **Dong S, Blissard GW.** 2012. Functional analysis of the *Autographa californica* multiple nucleopolyhedrovirus GP64 terminal fusion loops and interactions with membranes. J Virol **86:**9617–9628. http://dx.doi.org/10.1128/JVI.00813-12.
23. **Presti RM, Zhao G, Beatty WL, Mihindukulasuriya KA, da Rosa AP, Popov VL, Tesh RB, Virgin HW, Wang D.** 2009. Quaranfil, Johnston Atoll, and Lake Chad viruses are novel members of the family Orthomyxoviridae. J Virol **83:**11599–11606. http://dx.doi.org/10.1128/JVI.00677-09.
24. **Taylor RM, Hurlbut HS, Work TH, Kingston JR, Hoogstraal H.** 1966. Arboviruses isolated from Argas ticks in Egypt: Quaranfil, Chenuda, and Nyamanini. Am J Trop Med Hyg **15:**76–86.
25. **Clifford CM, Thomas LA, Hughes LE, Kohls GM, Philip CB.** 1968. Identification and comparison of two viruses isolated from ticks of the genus *Ornithodoros*. Am J Trop Med Hyg **17:**881–885.
26. **Kemp GE, Lee VH, Moore DL.** 1975. Isolation of Nyamanini and Quaranfil viruses from Argas (Persicargas) arboreus ticks in Nigeria. J Med Entomol **12:**535–537.
27. **Converse JD, Moussa MI.** 1982. Quaranfil virus from Hyalomma dromedarii (Acari: Ixodoidea) collected in Kuwait, Iraq and Yemen. J Med Entomol **19:**209–210.
28. **Yunker CE.** 1975. Tick-borne viruses associated with seabirds in North America and related islands. Med Biol **53:**302–311.
29. **Doherty RL, Whitehead RH, Wetters EJ, Johnson HN.** 1969. Isolation of viruses from Ornithodoros capensis Neumann from a tern colony on the Great Barrier Reef, north Queensland. Aust J Sci **31:**363–364.
30. **Austin FJ.** 1978. Johnston Atoll virus (Quaranfil group) from Ornithodoros capensis (Ixodoidea: Argasidae) infesting a gannet colony in New Zealand. Am J Trop Med Hyg **27:**1045–1048.

31. **Duffy DC.** 1983. The ecology of tick parasitism on densely nesting Peruvian seabirds. Ecology **64:**110–119. http://dx.doi.org/10.2307/1937334.
32. **Dietrich M, Gómez-Díaz E, McCoy KD.** 2011. Worldwide distribution and diversity of seabird ticks: implications for the ecology and epidemiology of tick-borne pathogens. Vector Borne Zoonotic Dis **11:**453–470. http://dx.doi.org/10.1089/vbz.2010.0009.
33. **Kaiser MN.** 1966. Viruses in ticks. I. Natural infections of Argas (Persicargas) arboreus by Quaranfil and Nyamanini viruses and absence of infections in A. (p.) persicus in Egypt. Am J Trop Med Hyg **15:**964–975.
34. **Kessell A, Hyatt A, Lehmann D, Shan S, Crameri S, Holmes C, Marsh G, Williams C, Tachedjian M, Yu M, Bingham J, Payne J, Lowther S, Wang J, Wang LF, Smith I.** 2012. Cygnet River virus, a novel orthomyxovirus from ducks, Australia. Emerg Infect Dis **18:**2044–2046. http://dx.doi.org/10.3201/eid1812.120500.
35. **Tesh RB, Travassos da Rosa AP, Travassos da Rosa JS.** 1983. Antigenic relationship among rhabdoviruses infecting terrestrial vertebrates. J Gen Virol **64:**169–176. http://dx.doi.org/10.1099/0022-1317-64-1-169.
36. **Shaw ML, Stone KL, Colangelo CM, Gulcicek EE, Palese P.** 2008. Cellular proteins in influenza virus particles. PLoS Pathog **4:**e1000085. http://dx.doi.org/10.1371/journal.ppat.1000085.
37. **Zerbino DR, Birney E.** 2008. Velvet: algorithms for de novo short read assembly using de Bruijn graphs. Genome Res **18:**821–829. http://dx.doi.org/10.1101/gr.074492.107.
38. **Peng Y, Leung HC, Yiu SM, Chin FY.** 2012. IDBA-UD: a de novo assembler for single-cell and metagenomic sequencing data with highly uneven depth. Bioinformatics **28:**1420–1428. http://dx.doi.org/10.1093/bioinformatics/bts174.
39. **Kuchibhatla DB, Sherman WA, Chung BY, Cook S, Schneider G, Eisenhaber B, Karlin DG.** 2014. Powerful sequence similarity search methods and in-depth manual analyses can identify remote homologs in many apparently "orphan" viral proteins. J Virol **88:**10–20. http://dx.doi.org/10.1128/JVI.02595-13.
40. **Hochrainer K, Racchumi G, Zhang S, Iadecola C, Anrather J.** 2012. Monoubiquitination of nuclear RelA negatively regulates NF-kB activity independent of proteasomal degradation. Cell Mol Life Sci **69:**2057–2073. http://dx.doi.org/10.1007/s00018-011-0912-2.
41. **Kelley LA, Sternberg MJ.** 2009. Protein structure prediction on the Web: a case study using the Phyre server. Nat Protoc **4:**363–371. http://dx.doi.org/10.1038/nprot.2009.2.
42. **Harlow E, Lane D.** 1999. Using antibodies: a laboratory manual. Cold Spring Harbor Laboratory Press, Cold Spring Harbor, NY.
43. **Lin DA, Roychoudhury S, Palese P, Clay WC, Fuller FJ.** 1991. Evolutionary relatedness of the predicted gene-product of RNA segment-2 of the tick-borne Dhori virus and the PB1 polymerase gene of influenza-viruses. Virology **182:**1–7. http://dx.doi.org/10.1016/0042-6822(91)90641-N.
44. **Edgar RC.** 2004. MUSCLE: a multiple sequence alignment method with reduced time and space complexity. BMC Bioinformatics **5:**113. http://dx.doi.org/10.1186/1471-2105-5-113.
45. **Talavera G, Castresana J.** 2007. Improvement of phylogenies after removing divergent and ambiguously aligned blocks from protein sequence alignments. Syst Biol **56:**564–577. http://dx.doi.org/10.1080/10635150701472164.
46. **Guindon S, Dufayard JF, Lefort V, Anisimova M, Hordijk W, Gascuel O.** 2010. New algorithms and methods to estimate maximum-likelihood phylogenies: assessing the performance of PhyML 3.0. Syst Biol **59:**307–321. http://dx.doi.org/10.1093/sysbio/syq010.
47. **Lvov DK, Alkhovsky SV, Shchelkanov Yu M, Shchetinin AM, Deryabin PG, Aristova VA, Gitelman AK, Samokhvalov EI, Botikov AG.** 2014. Taxonomic status of the Tyulek virus (TLKV) (Orthomyxoviridae, Quaranjavirus, Quaranfil group) isolated from the ticks Argas vulgaris Filippova, 1961 (Argasidae) from the birds burrow nest biotopes in the Kyrgyzstan. Vopr Virusol **59:**28–32.
48. **Belrose F.** 1976. Ducks, geese and swans of North America. Stackpole Books, Harrisburg, PA.
49. **Desselberger U, Racaniello VR, Zazra JJ, Palese P.** 1980. The 3′ and 5′-terminal sequences of influenza A, B and C virus RNA segments are highly conserved and show partial inverted complementarity. Gene **8:**315–328. http://dx.doi.org/10.1016/0378-1119(80)90007-4.
50. **Biswas SK, Nayak DP.** 1994. Mutational analysis of the conserved motifs of influenza A virus polymerase basic protein 1. J Virol **68:**1819–1826.
51. **Shaw ML, Palese P.** 2013. Orthomyxoviridae, p 1151–1185. *In* Knipe DM, Howley PM (ed), Fields virology, 6th ed. Lippincott Williams and Wilkins, Philadelphia, PA.
52. **Ye Z, Robinson D, Wagner RR.** 1995. Nucleus-targeting domain of the matrix protein (M1) of influenza virus. J Virol **69:**1964–1970.
53. **Paterson D, Fodor E.** 2012. Emerging roles for the influenza A virus nuclear export protein (NEP). PLoS Pathog **8:**e1003019. http://dx.doi.org/10.1371/journal.ppat.1003019.
54. **la Cour T, Gupta R, Rapacki K, Skriver K, Poulsen FM, Brunak S.** 2003. NESbase version 1.0: a database of nuclear export signals. Nucleic Acids Res **31:**393–396. http://dx.doi.org/10.1093/nar/gkg101.
55. **Diaz J-J, Roufa DJ.** 1992. Fine-structure map of the human ribosomal protein gene RPS14. Mol Cell Biol **12:**1680–1686.
56. **Ferreira-Cerca S, Poll G, Gleizes PE, Tschochner H, Milkereit P.** 2005. Roles of eukaryotic ribosomal proteins in maturation and transport of pre-18S rRNA and ribosome function. Mol Cell **20:**263–275. http://dx.doi.org/10.1016/j.molcel.2005.09.005.
57. **Zhou X, Hao Q, Liao J, Zhang Q, Lu H.** 2013. Ribosomal protein S14 unties the MDM2-p53 loop upon ribosomal stress. Oncogene **32:**388–396. http://dx.doi.org/10.1038/onc.2012.63.
58. **Zhou X, Hao Q, Liao JM, Liao P, Lu H.** 2013. Ribosomal protein S14 negatively regulates c-Myc activity. J Biol Chem **288:**21793–21801. http://dx.doi.org/10.1074/jbc.M112.445122.
59. **Oh ES, Woods S, Couchman JR.** 1997. Multimerization of the cytoplasmic domain of syndecan-4 is required for its ability to activate protein kinase C. J Biol Chem **272:**11805–11811.
60. **Lefèvre M, Felmlee DJ, Parnot M, Baumert TF, Schuster C.** 2014. Syndecan 4 is involved in mediating HCV entry through interaction with lipoviral particle-associated apolipoprotein E. PLoS One **9:**e95550. http://dx.doi.org/10.1371/journal.pone.0095550.
61. **Zinn AR, Alagappan RK, Brown LG, Wool I, Page DC.** 1994. Structure and function of ribosomal protein S4 genes on the human and mouse sex chromosomes. Mol Cell Biol **14:**2485–2492. http://dx.doi.org/10.1128/MCB.14.4.2485.
62. **Monsma SA, Blissard GW.** 1995. Identification of a membrane fusion domain and an oligomerization domain in the baculovirus GP64 envelope fusion protein. J Virol **69:**2583–2595.
63. **Li Z, Blissard GW.** 2011. Autographa californica multiple nucleopolyhedrovirus gp64 protein: roles of histidine residues in triggering membrane fusion and fusion pore expansion. J Virol **85:**12492–12504. http://dx.doi.org/10.1128/JVI.05153-11.
64. **Zeller HG, Karabatsos N, Calisher CH, Digoutte JP, Murphy FA, Shope RE.** 1989. Electron microscopy and antigenic studies of uncharacterized viruses. I. Evidence suggesting the placement of viruses in families Arenaviridae, Paramyxoviridae, or Poxviridae. Arch Virol **108:**191–209.
65. **Yunker CE, Clifford CM, Keirans JE, Thomas LA, Rice RCA.** 1979. Aransas Bay virus, a new arbovirus of the Upolu serogroup from Ornithodoros capensis (Acari: Argasidae) in coastal Texas. J Med Ent **16:**453–460.
66. **Frese M, Weeber M, Weber F, Speth V, Haller O.** 1997. Mx1 sensitivity: Batken virus is an orthomyxovirus closely related to Dhori virus. J Gen Virol **78:**2453–2458.
67. **Da Silva EV, Da Rosa AP, Nunes MR, Diniz JA, Tesh RB, Cruz AC, Vieira CM, Vasconcelos PF.** 2005. Araguari virus, a new member of the family Orthomyxoviridae: serologic, ultrastructural, and molecular characterization. Am J Trop Med Hyg **73:**1050–1058.
68. **Bussetti AV, Palacios G, Travassos da Rosa A, Savji N, Jain K, Guzman H, Hutchison S, Popov VL, Tesh RB, Lipkin WI.** 2012. Genomic and antigenic characterization of Jos virus. J Gen Virol **93:**293–298. http://dx.doi.org/10.1099/vir.0.035121-0.
69. **Briese T, Chowdhary R, Travassos da Rosa A, Hutchison SK, Popov V, Street C, Tesh RB, Lipkin WI.** 2014. Upolu virus and Aransas Bay virus, two presumptive bunyaviruses, are novel members of the family Orthomyxoviridae. J Virol **88:**5298–5309. http://dx.doi.org/10.1128/JVI.03391-13.
70. **Levin BR.** 1996. The evolution and maintenance of virulence in microparasites. Emerg Infect Dis **2:**93–102. http://dx.doi.org/10.3201/eid0202.960203.
71. **Rabl J, Leibundgut M, Ataide SF, Haag A, Ban N.** 2011. Crystal structure of the eukaryotic 40S ribosomal subunit in complex with initiation factor 1. Science **331:**730–736. http://dx.doi.org/10.1126/science.1198308.
72. **Ebert BL, Pretz J, Bosco J, Chang CY, Tamayo P, Galili N, Raza A, Root DE, Attar E, Ellis SR, Golub TR.** 2008. Identification of RPS14 as a 5q-syndrome gene by RNA interference screen. Nature **451:**335–359. http://dx.doi.org/10.1038/nature06494.
73. **Cheng E, Haque A, Rimmer MA, Hussein IT, Sheema S, Little A, Mir MA.** 2011. Characterization of the interaction between hantavirus nucleo-

capsid protein (N) and ribosomal protein S19 (RPS19). J Biol Chem **286:** 11814–11824. http://dx.doi.org/10.1074/jbc.M110.210179.

74. **Lee AS, Burdeinick-Kerr R, Whelan SP.** 2013. A ribosome-specialized translation initiation pathway is required for cap-dependent translation of vesicular stomatitis virus mRNAs. Proc Natl Acad Sci U S A **110:**324–329. http://dx.doi.org/10.1073/pnas.1216454109.
75. **Bernstein KA, Gallagher JE, Mitchell BM, Granneman S, Baserga SJ.** 2004. The small-subunit processome is a ribosome assembly intermediate. Eukaryot Cell **3:**1619–1626. http://dx.doi.org/10.1128/EC.3.6.1619-1626.2004.
76. **Sudhamalla B, Yadaiah M, Ramakrishna D, Bhuyan AK.** 2012. Cysteine protease attribute of eukaryotic ribosomal protein S4. Biochim Biophys Acta **1820:**1535–1542. http://dx.doi.org/10.1016/j.bbagen.2012.05.001.
77. **Staunton D, Nuttall PA, Bishop DH.** 1989. Sequence analyses of Thogoto viral RNA segment 3: evidence for a distant relationship between an arbovirus and members of the Orthomyxoviridae. J Gen Virol **70:**2811–2817. http://dx.doi.org/10.1099/0022-1317-70-10-2811.
78. **Reeves WK, Loftis AD, Sanders F, Spinks MD, Wills W, Denison AM, Dasch GA.** 2006. Borrelia, Coxiella, and Rickettsia in Carios capensis (Acari: Argasidae) from a brown pelican (Pelecanus occidentalis) rookery in South Carolina, USA. Exp Appl Acarol **39:**321–329. http://dx.doi.org/10.1007/s10493-006-9012-7.
79. **Smith RP, Jr, Muzaffar SB, Lavers J, Lacombe EH, Cahill BK, Lubelczyk CB, Kinsler A, Mathers AJ, Rand PW.** 2006. Borrelia garinii in seabird ticks (Ixodes uriae), Atlantic Coast, North America. Emerg Infect Dis **12:** 1909–1912. http://dx.doi.org/10.3201/eid1212.060448.
80. **St. George TD, Doherty RL, Carley JG, Filippich C, Brescia A, Casals J, Kemp DH, Brothers N.** 1985. The isolation of arboviruses including a new flavivirus and a new Bunyavirus from Ixodes (Ceratixodes) uriae (Ixodoidea: Ixodidae) collected at Macquarie Island, Australia, 1975–1979. Am J Trop Med Hyg **34:**406–412.
81. **Labuda M, Nuttall PA.** 2004. Tick-borne viruses. Parasitology **129:**S221–S245. http://dx.doi.org/10.1017/S0031182004005220.
82. **Major L, Linn ML, Slade RW, Schroder WA, Hyatt AD, Gardner J, Cowley J, Suhrbier A.** 2009. Ticks associated with Macquarie Island penguins carry arboviruses from four genera. PLoS One **4:**e4375. http://dx.doi.org/10.1371/journal.pone.0004375.
83. **Heath ACG.** 1987. A review of the origins and zoogeography of tick-borne disease in New Zealand. Tuatara **29:**19–29.
84. **Shaffer SA, Tremblay Y, Weimerskirch H, Scott D, Thompson DR, Sagar PM, Moller H, Taylor GA, Foley DG, Block BA, Costa DP.** 2006. Migratory shearwaters integrate oceanic resources across the Pacific Ocean in an endless summer. Proc Natl Acad Sci U S A **103:**12799–12802. http://dx.doi.org/10.1073/pnas.0603715103.